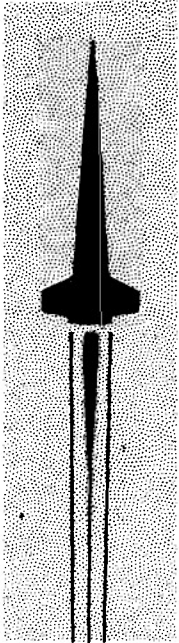


MIRADCOM 7-1R-79-42

Cy 11 RB 21



TECHNICAL REPORT T-79-42

FINAL EVALUATION OF RAIN EROSION SLED
TEST RESULTS AT MACH 3.7 TO 5.0 FOR SLIP-
CAST FUSED SILICA RADOME STRUCTURES

**U.S. ARMY
MISSILE
RESEARCH
AND
DEVELOPMENT
COMMAND**

Kenneth N. Letson
William G. Burleson
Technology Laboratory

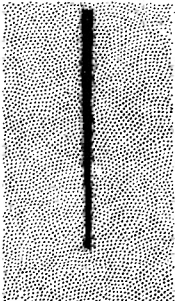
LOAN COPY ONLY - DO NOT DESTROY
PROPERTY OF
REDSTONE SCIENTIFIC INFORMATION CENTER
NOV 21 1979



6 March 1979

Redstone Arsenal, Alabama 35809

Approved for Public Release Distribution Unlimited.



REDSTONE SCIENTIFIC INFORMATION CENTER



5 0510 00266767 0

DISPOSITION INSTRUCTIONS

DESTROY THIS REPORT WHEN IT IS NO LONGER NEEDED. DO NOT RETURN IT TO THE ORIGINATOR.

DISCLAIMER

THE FINDINGS IN THIS REPORT ARE NOT TO BE CONSTRUED AS AN OFFICIAL DEPARTMENT OF THE ARMY POSITION UNLESS SO DESIGNATED BY OTHER AUTHORIZED DOCUMENTS.

TRADE NAMES

USE OF TRADE NAMES OR MANUFACTURERS IN THIS REPORT DOES NOT CONSTITUTE AN OFFICIAL ENDORSEMENT OR APPROVAL OF THE USE OF SUCH COMMERCIAL HARDWARE OR SOFTWARE.

Unclassified

SECURITY CLASSIFICATION OF THIS PAGE (When Data Entered)

REPORT DOCUMENTATION PAGE		READ INSTRUCTIONS BEFORE COMPLETING FORM
1. REPORT NUMBER T-79-42	2. GOVT ACCESSION NO.	3. RECIPIENT'S CATALOG NUMBER
4. TITLE (and Subtitle) Final Evaluation of Rain Erosion Sled Test Results at Mach 3.7 to 5.0 for Slip-Cast Fused Silica Radome Structures		5. TYPE OF REPORT & PERIOD COVERED Technical Report
		6. PERFORMING ORG. REPORT NUMBER
7. AUTHOR(s) Kenneth N. Letson William G. Burleson		8. CONTRACT OR GRANT NUMBER(s)
9. PERFORMING ORGANIZATION NAME AND ADDRESS Commander US Army Missile Command ATTN: DRSMI-TL (R&D) Redstone Arsenal, Alabama 35809		10. PROGRAM ELEMENT, PROJECT, TASK AREA & WORK UNIT NUMBERS
11. CONTROLLING OFFICE NAME AND ADDRESS Commander US Army Missile Command ATTN: DRSMI-TI (R&D) Redstone Arsenal, Alabama 35809		12. REPORT DATE 6 March 1979
		13. NUMBER OF PAGES 62
14. MONITORING AGENCY NAME & ADDRESS (if different from Controlling Office)		15. SECURITY CLASS. (of this report) Unclassified
		15a. DECLASSIFICATION/DOWNGRADING SCHEDULE
16. DISTRIBUTION STATEMENT (of this Report) Approved for public release; distribution unlimited.		
17. DISTRIBUTION STATEMENT (of the abstract entered in Block 20, if different from Report)		
18. SUPPLEMENTARY NOTES		
19. KEY WORDS (Continue on reverse side if necessary and identify by block number) Radome Erosion Supersonic Rain Erosion Rain Erosion Slip-Cast Fused Silica Ceramic Radomes Sled Tests in Rain		
20. ABSTRACT (Continue on reverse side if necessary and identify by block number) This report contains a summary of rain erosion results obtained for high-purity slip-cast fused silica (SCFS) models on sleds at Holloman Air Force Base, New Mexico. This effort, which was initiated to evaluate the rain erosion behavior of SCFS as a function of velocity and angle of incidence was completed with good correlation of results. The tests were performed in artificial rain at average velocities between 1270 and 1740 m/sec (Mach 3.7 and 5.0). Right circular cone models having semivertex angles of 15, 19, 22.5, 25, 27.5, and 30 degrees were tested.		

A special test vehicle and sample design were utilized to avoid sled vibration-induced failures that are common to small samples of brittle ceramics at velocities near Mach 5. A unique feature of the sled test vehicle is its capability of testing seven cone frusta, thereby simulating actual radome forebody shapes. The sample design and special mounting technique resulted in obtaining correlatable erosion data which were free of spurious mass losses caused by sample fracture and edge effects.

Because SCFS has low fracture toughness and relatively poor rain erosion resistance under severe conditions, other candidate ceramic and plastic radome materials were tested concurrently in the interest of finding a tougher structure. However only those results for SCFS are presented in this report.

The major observations from the rain erosion tests on SCFS are:

1. The scatter in the measured maximum erosion rate of SCFS was less than a factor of three for the same normal component of velocity. This behavior is considered normal due to the brittleness of SCFS and the variability of the rainfield.
2. The rain erosion threshold or discontinuity in the erosion rate profile for high-purity SCFS (density = $1.95 \pm .03$ g/cc) occurs at a normal component of velocity of approximately 500 m/sec for rainfields equivalent to the artificial rainfield at Holloman Air Force Base.
3. At a normal component of velocity above the threshold region, the risk of catastrophic failure of an SCFS radome is unacceptably high. Therefore, flight limitations in terms of velocity and impingement angles can be established for a specific rainfield.
4. Silicone resin moisture sealants DC808 and GE SR80 probably do not significantly affect the rain erosion behavior of SCFS.

ACKNOWLEDGMENT

The authors express appreciation for the support and cooperation of all personnel who contributed to the accomplishment of this effort: Mr. Phil Ormsby and other personnel in the materials section of the US Army Missile Research and Development Command (MIRADCOM) who provided samples and participated in the testing; Mr. T. S. King and many shop personnel for fabrication of the test vehicle and finishing the test samples; Mr. R. A. Reynolds for thermal analyses and technical consultations; and Mr. Berle E. Engle (Test Manager) and other personnel of the 6585 Track Test Group, who performed the tests and recorded the data.



CONTENTS

Section	Page
1. Introduction	5
2. Test Program	6
3. Rain Erosion Sled Test Results	6
A. Summary of Tests 1 through 5	9
B. Test 7	10
C. Test 8	10
D. Test 10	10
E. Test 11	11
4. Discussion of Sled Test Results	11
5. Conclusions and Recommendations	13
Appendix A. Test Vehicle Description	43
Appendix B. Test Specimen Subassembly	47
Appendix C. Test Facility	51
Appendix D. Test Environment	53
References	59



ILLUSTRATIONS

Figure	Page
1. Test Vehicle and Sample Orientation	7
2. Sample Subassembly for Initial Test	8
3. Samples Assembled for Test 1	20
4. Post-Test View of Test Vehicle and Samples of Test 1	21
5. Samples Assembled for Test 2	22
6. Mach 5 Shocks on Samples in Test 2	23
7. Test Vehicle and Samples After Test 2	24
8. Samples Assembled for Test 3	25
9. Test Vehicle and Samples After Test 3	26
10. Samples Assembled for Test 4	27
11. Test Vehicles and Samples After Test 4	28
12. Samples Assembled for Test 5	29
13. Test Vehicle and Samples After Test 5	30
14. Modifications to Sample Subassembly for Test 5 and Subsequent Tests	31
15. Samples Assembled for Test 8	32

ILLUSTRATIONS (CONCLUDED)

Figure	Page
16. Test Vehicle and Samples After Test 8	33
17. Samples Assembled for Test 10	34
18. Test Vehicle and Samples After Test 10	35
19. Samples Assembled for Test 11	36
20. Test Vehicle and Samples After Test 11	37
21. Rain Erosion Results for Bare SCFS on Supersonic Sleds	38
22. Rain Erosion Results for Bare SCFS on Supersonic Sleds	39
23. Measured Maximum Erosion Rate of SCFS	40
24. Allowable Angle-of-Impingement for SCFS	41
A-1. Test Vehicle Assembly	44
A-2. Test Vehicle	45
B-1. Typical Result From First Test	49
C-1. Test Vehicle and Sled Assembly	52
D-1. Holloman Rainfield	54
D-2. Rainfield Drop Size Distribution	55
D-3. Sled Velocity in the Rainfield	56
D-4. Calculated Temperature Histories of SCFS in a Mach 5 Sled Test	58

1. INTRODUCTION

The important parameters which influence the rain erosion behavior of a material can be classified as:

- Those which relate to the environment such as drop size, drop size distribution, and liquid water content of the air.
- Those which relate to the geometry of the material exposed to rain such as angle of impingement and surface roughness.
- Those which relate to the properties of the material such as microstructure, density, porosity, acoustic velocity, modulus of elasticity, strength, and hardness.

The temperature distribution through the radome material at entrance to the rainfield is an additional factor which is important for some flight regimes. Therefore, it is important that a material be properly characterized because of the wide possible variability of properties.

For a particular material, the more important parameters involved in rain erosion are drop size, number of encounters, velocity of impact, and angle of impact. The temperature of the material becomes more important in direct relation to its effect on mechanical properties.

The most widely used test facility capable of testing radome materials in multiple impact simulated rain at Mach 5 is the monorail sled facility at the Holloman Air Force Base, New Mexico. In the current Holloman rainfield, the median volume diameter drop size is approximately 1.4 mm. Surveys of natural rain indicate that median volume diameters range from approximately 1.0 to 2.0 mm in the temperate climatic regions.¹ By this measure the Holloman rainfield provides a reasonable simulation of natural rain.

The number of raindrops that encounter the test item depends on the density and length of the rainfield. The rain density is referred to as the liquid water content and is usually expressed in grams of water per cubic meter of air. To a first approximation the number of raindrops that encounter a surface in flight can be simulated in an artificial rainfield by shortening the length of the field and increasing the rain density proportionately.² The mean density of the current Holloman rainfield is 3.1 g/m^3 . The resulting mean rain rate is 67 mm/hr, which is 21.5 mm/hr for each g/m^3 of rainfield density. The corresponding ratio for natural rain is 23.2 mm/hr per g/m^3 of rainfield density.²

Previous efforts to evaluate the rain erosion behavior of slip-cast fused silica (SCFS) at supersonic velocities are well documented.³⁻⁵ However, prior to the tests

discussed herein, rain erosion data for natural high-purity SCFS had not been generated. The high-purity silica is usually sintered to a higher density (lower porosity) to achieve higher strength. The increased strength does not necessarily improve its resistance to damage by rain. In fact, Walton, et al.⁶ found that in the fully dense condition, SCFS is more susceptible to catastrophic fracture at velocities near Mach 5 than is the lower-density material, which erodes in layers. However, at velocities below Mach 3 the higher-density material experiences less erosion. It is generally assumed that the SCFS of higher porosity more successfully prevents the propagation of cracks because the pores tend to stop crack propagation.

Because SCFS is porous and hygroscopic, sealing against moisture absorption is necessary to prevent electrical and structural degradation: electrical through change in dielectric constant and structural through possible surface spallation in flight at elevated temperature.

2. TEST PROGRAM

The primary purpose of this effort was to determine the rain erosion behavior of high-purity SCFS as a function of velocity and angle of incidence. A second objective was to determine if the coating/impregnant utilized to minimize moisture absorption had any effect on the erosion behavior of the SCFS. A third objective was to screen radome materials for use in flight regimes of Mach 4 to 6.

The program involved testing cone frusta samples of SCFS in the artificial rainfield on supersonic sleds at Holloman Air Force Base. One to seven SCFS samples were tested on each of nine sled runs. Models having semivertex angles of 15, 19, 22.5, 25, 27.5 and 30 deg were tested. Average velocities in the rainfield were 1272, 1433, 1524, and 1710 m/sec (Mach 3.7, 4.2, 4.5, 5.0).

Figure 1 shows the test vehicle with sample subassemblies that were developed for this effort. The test vehicle designs⁷ and fabrication are discussed in Appendix A. A sketch of the initial subassembly design is presented in *Figure 2*. Appendices B, C, and D show the design and modification, the Holloman sled test facility, and test environment, respectively.

3. RAIN EROSION SLED TEST RESULTS

A summary of sample performance in all tests is presented in *Table 1*. Samples are identified by test number-position number. Position number refers to position on the test vehicle numbered clockwise facing the vehicle and beginning at the 1 o'clock position as indicated in *Figure 1*. Position 7 is in the center as shown. To evaluate the behavior of the materials, surface profile measurements, before and after each test, were made at several positions on each sample with a precision profilometer. Also, the samples were weighed before and after the tests. The maximum depth of penetration, maximum depth of penetration

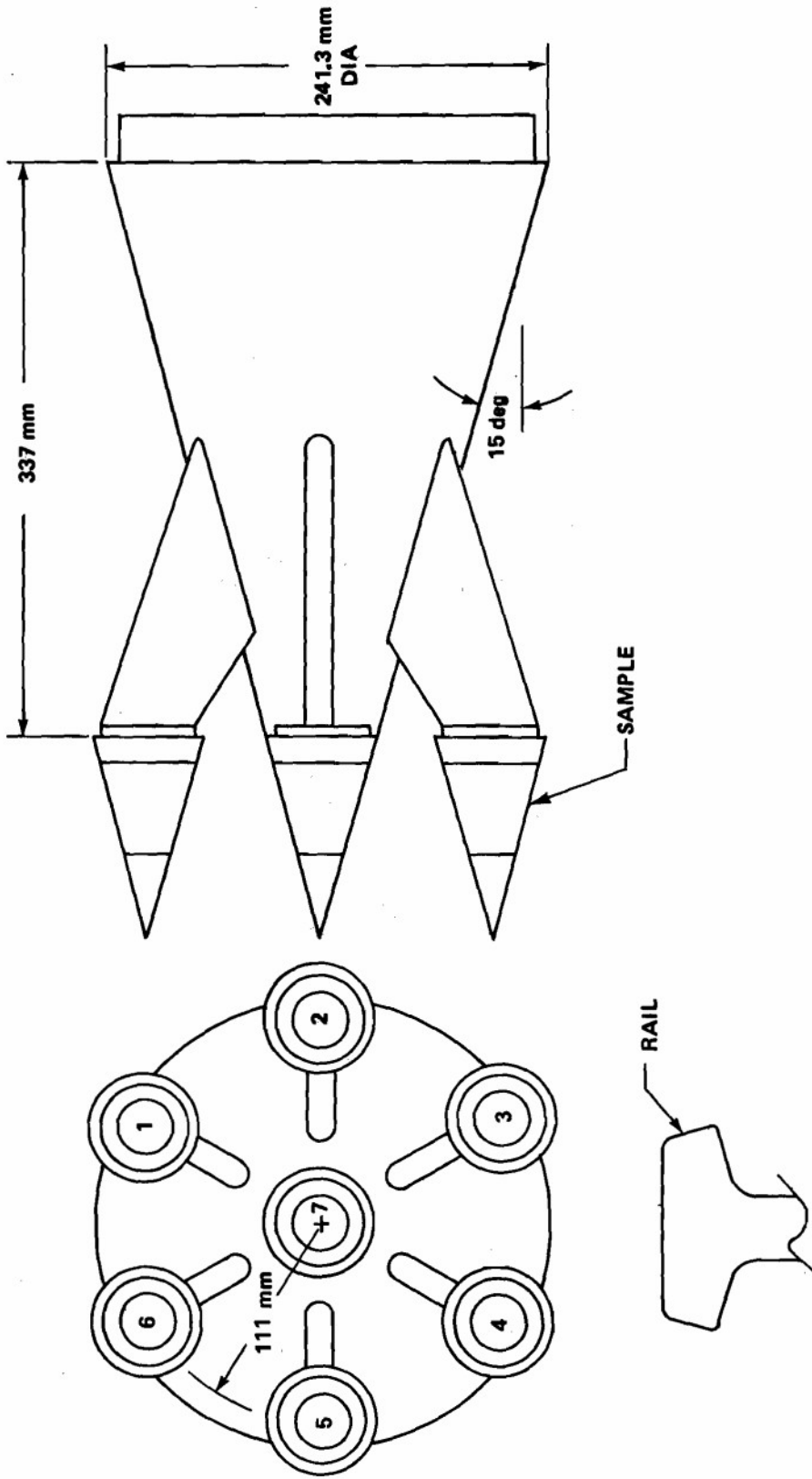


Figure 1. Test vehicle and sample orientation.

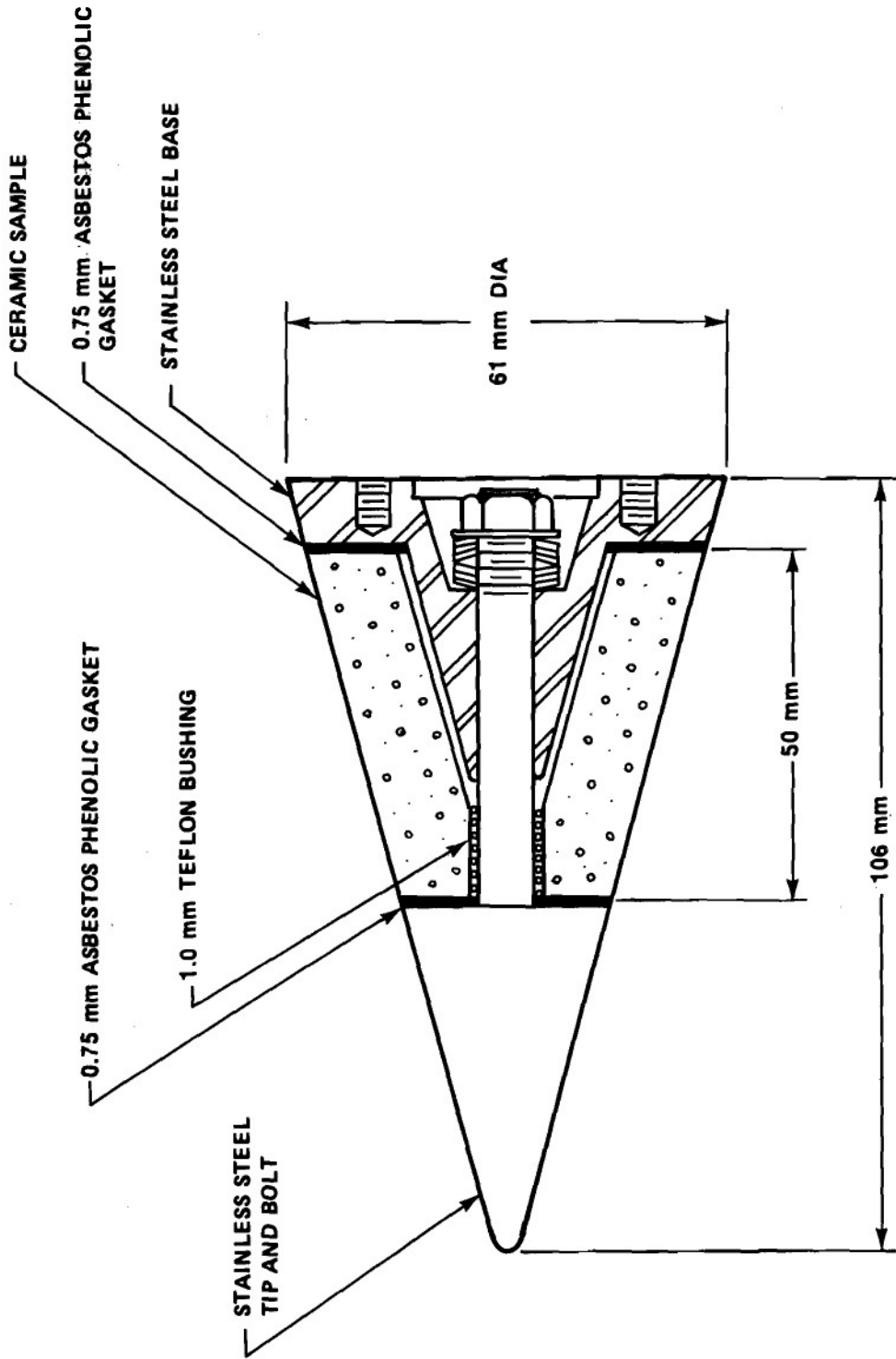


Figure 2. Sample subassembly for initial test.

rate, and average depth of penetration rate are reported in *Table 1*. The average depth of penetration rate is defined by the expression:

$$\text{Average Depth of Penetration Rate} = \frac{\text{Weight Loss}}{\text{Material Density} \times \text{Effective Surface Area} \times \text{Time in Rain}}$$

The maximum depth of penetration rate is found by dividing the maximum depth of penetration (measured by the profilometer) by the time in rain (*Table 2*). Maximum erosion depths and rates are considered to be of most interest and value, because erosion was not uniform over the surface of any sample, and radome structural failure or radar attenuation can be expected to occur or be worst where erosion is worst. Because initiation of erosion depends on raindrop size, and erosion rate depends on surface roughness, it follows that areas which experience early impact by large drops would sustain the greater erosion.

The center models (samples) on tests 8, 10, and 11 were equipped with a steel raincap having a tip diameter of 19.05 mm. All other samples had a raincap tip diameter of 3.175 mm. The raincap of the center sample was blunted to cause the shock waves to intersect farther from the conical test vehicle and the model-holding struts, thereby reducing shock-impingement heating to the test vehicle structure. While traversing the rainfield, shock waves from the models intersect well aft of the models, thus eliminating shock interaction on adjacent samples. Rain damage to SCFS appears to have been insensitive to differences in the two raincap nose radii used.

A. SUMMARY OF TESTS 1 THROUGH 5

Complete results for the first five sled tests are covered in reference 7 and are summarized here. Test conditions and results for the first five sled tests are listed in *Tables 1* and *2*. During this initial phase of the test program, a model design and mounting technique were developed that prevented or minimized ceramic sample damage and loss due to spurious causes (sled vibration and stress risers caused by sample size, shape, and edges). In spite of these problems, more than two-thirds of the SCFS samples tested provided good correlatable erosion data. In addition to bare SCFS, SCFS with moisture sealants and a few other candidate radome materials were tested.

Figure 3 through *13* are pre- and post-test photographs of the test specimen and hardware for the first five tests. The SCFS samples in *Figure 4* show the detrimental effects of sharp edges at the base for the sample design of *Figure 2*. All samples with a semivertex angle of 15 deg survived the 610 m rainfield at Mach 5 with negligible erosion because the normal component of velocity ($V \sin \theta$) was less than that at which significant erosion begins on SCFS.

Edge effects in the form of chipping at the base in test 1 were eliminated in test 2 and subsequent tests by redesigning the external configuration of the ceramic sample as shown in *Figure 14*. All samples were SCFS in test 2 except sample 5, which was Avcoat

8027, an epoxy. Only the 22.5 deg center sample and the 15 deg sample coated with chromium oxide (sample 1) were lost in the 1100 m rainfield. Erosion of high-purity SCFC (samples 2, 3, and 4) was very minor, whereas the erosion of low-density SCFS (sample 6) was great.

In test 3 only one SCFS model (15 deg in *Figure 9*) survived at Mach 5 through 853 m of artificial rain. The other 15 deg sample was lost after exit from the rainfield. All 22.5 deg models were lost. A ruptured water line, which possibly sprayed water across the track, may have contributed to sample failures in this test. The center sample was Avcoat 8027.

Teflon, Avcoat 8027, and hot-pressed silicon nitride survived in test 4. One SCFS sample was lost early in the rainfield (evidenced by the severity of rain damage on sample mounting hardware), two samples were damaged in rain, and the remaining material was lost after leaving the rainfield. One SCFS sample (4-1, *Figure 11*) survived in a severely damaged condition. Additional shock mounting procedures (Appendix B) were implemented for SCFS samples with semivertex angles of 22.5 deg and greater to prevent sample loss after severe erosion.

Beginning with test 5, the techniques used to eliminate damage by track vibrations and stress risers were successful so that all subsequent samples of SCFS were recovered in a condition which allowed correlations to be made between erosion, velocity, and angle of impingement. Six

SCFS specimens were successfully tested on test 5 (*Figure 13*). The center sample was made of quartz-polyimide.

B. TEST 7 (52R-A2)

Sample 2 was the only SCFS model in test 7. This 22.5 deg specimen was tested at an average velocity of 1727 m/sec (5666 ft/sec) in rain. Its performance (*Table 1*) was very similar to that of SCFS samples with the same semivertex angle and density tested previously.⁷

C. TEST 8 (52R-B2)

Table 1 gives characterization and performance data for each sample in test 8. The cone semivertex angles were 19, 22.5 and 25 deg and the average velocity in the rainfield (*Table 2*) was 1524 m/sec (5000 ft/sec). A pretest view of the test vehicle and samples is shown in *Figure 15* and the post-test view is found in *Figure 16*. The surface condition and weight loss of sample 8-4 indicate that a rain damage/erosion threshold occurs at a normal component of velocity near 500 m/sec; i.e., while most of the surface was covered with very small pits, a few large craters were found.

D. TEST 10 (52R-C1)

The excellent results from test 8 completed the data requirements at a velocity near Mach 5. Data at lower velocities and greater impingement angles were needed to determine if the dependence of erosion on the normal component of

velocity holds at other conditions. An average velocity in rain of 1272 m/sec (4175 ft/sec) was achieved in test 10, which included seven SCFS samples with semivertex angles of 25, 27.5, and 30 deg. Erosion data (mass loss, profilometer measurements, and visual inspections) from this test correlate well with previous results and further substantiate the conclusion that the erosion threshold velocity occurs near 500 m/sec.

Pre- and post-test views of the test vehicle and samples are shown in *Figures 17 and 18*. The center sample (10-7) had a 25 deg semivertex angle which caused its normal component of velocity to be slightly above the damage threshold region as indicated by visual inspection and the measured mass loss of 1.175 g (*Table 1*). Erosion data from all seven samples correlated well with previous results.

E. TEST 11 (52R-D1)

The sled velocity for test 11 was selected to provide additional data at a velocity between those of tests 8 and 10. Results from these two previous tests indicated that samples with semivertex angles of 22.5, 25, and 27.5 deg should be tested. Six SCFS samples (*Figure 19*) were tested in test 11: one of 22.5 deg, three of 25 deg, and two of 27.5 deg. The seventh sample on this test (11-1) was a silica-filled, filament-wound silica furnished by the Lockheed Missiles and Space Company, Inc.

The normal component of velocity (548 m/sec) of the 22.5 deg SCFS sample was near the damage threshold value (500 m/sec) as indicated by earlier results in this test series, and the performance of this sample was consistent with the previous results. The rain erosion data from all SCFS samples in this test correlate well with data from the previous tests. Post-test views of the samples are found in *Figure 20*.

4. DISCUSSION OF SLED TEST RESULTS

Thirty-one "bare" SCFS samples with a density of $1.95 \pm 0.03 \text{ g/cm}^3$ were successfully tested in rain, as listed in *Table 3*. Pre- and post-test profilometer and weight measurements, as well as post-test structural appearance, indicate that the rain erosion effects on these samples vary with velocity and impingement angle.

Rain erosion data from the sled tests have been assessed from several viewpoints. Mass loss ratio, the ratio of material eroded to water encountered, is presented in *Figure 21*. Within the velocity range of the tests, a modified hyperbolic equation fits the data well. These data indicate that catastrophic damage may begin at a normal component of velocity slightly above 620 m/sec. Examination of samples, however, indicates unacceptable damage at lower velocities. When the experimental data are plotted on semilogarithmic paper (*Figure 22*), a discontinuity in the mass loss ratio is indicated at a normal component of velocity near 500 m/sec.

In addition, because maximum erosion depth is believed to be of much greater importance than mass loss or average erosion, the maximum erosion rate is also presented in *Figure 23*. This figure shows that, for a given normal component of velocity, the variation in the maximum erosion rate (MER) is no greater than a factor of three, a low value when the fragility of SCFS and the variability of the rainfield are considered.

The six data points shown for a normal component of velocity ($V \sin \theta$) near 440 m/sec were obtained from models with a semivertex angle of 15 deg. In addition, other samples with $\theta = 15$ deg were run with SR-80 impregnant, DC-808 coating, and Cr_2O_3 surface impregnant.⁷ The effects of these coatings/impregnants on rain erosion resistance appear to be negligible. The MER's for the remaining samples impregnated with SR-80 are slightly higher than the data for "bare" SCFS samples. However, the difference is not significant.

The data in *Figures 21, 22, and 23* alone do not fully indicate the significance of the discontinuity in the rain erosion rate profile of SCFS. These data, when taken in conjunction with visual inspections, reveal that the rain damage mechanism changes from one of erosion to one of cratering at the discontinuity, i.e., at the "rain damage threshold" near $V \sin \theta = 500$ m/sec. At normal velocities below this threshold, erosion was measurable but minimal, consisting of very minor pits which covered

almost the complete surface of the sample. At normal components of velocity near the threshold, there were, in addition to the minor pits, a few craters with volumes approximately 100 to 200 times those of the minor pits. Obviously the onset and size of cratering depend strongly on water droplet size also. This cratering behavior is believed representative of that caused by natural rain by virtue of the accuracy of the simulation.

As the normal component of velocity increases above the threshold value, the size and number of craters increase proportionately. Also at velocities slightly above the threshold value, some samples cracked. Thus the *major finding* in this effort was the identification of the damage threshold region for SCFS, above which rain erosion is expected to be severe and the risk of catastrophic failure of an SCFS radome is unacceptably high. Therefore, for rainfields equivalent to that at the Holloman Air Force Base, the maximum safe velocity for an SCFS radome occurs when the normal component of velocity is 500 m/sec.

Based on rain damage results from sled tests, the maximum allowable angle of impingement versus freestream velocity is shown in *Figure 24* for SCFS radomes. These data show that the radome angle-of-impingement should not exceed 15 deg at 1932 m/sec (6340 ft/sec), 20 deg at 1462 m/sec (4797 ft/sec), and 25 deg at 1183 m/sec (3880 ft/sec). The most accurate data are for freestream velocities above 1272

m/sec (4175 ft/sec), because the sled was run through rain at or above this average velocity. The extrapolation of the data in *Figure 24* to lower velocities and higher angles as shown is believed satisfactory for flights of short duration.

5. CONCLUSIONS AND RECOMMENDATIONS

1. The measured maximum erosion rate for SCFS tested at the Holloman Air Force Base sled track facility varied by a factor of three for the same normal component of velocity. This behavior is considered normal because of the brittleness of SCFS and the variability of the rainfield.

2. The rain erosion threshold or discontinuity in the erosion rate profile for high-purity SCFS (density = 1.95 ± 0.03 g/cm³) occurs at a normal component of

velocity of approximately 500 m/sec for rainfields equivalent to the artificial rainfield at Holloman Air Force Base.

3. At a normal component of velocity above the threshold region, the risk of catastrophic failure of an SCFS radome is unacceptably high.

4. Silicone resin moisture sealants DC808 and GE SR80 probably do not significantly affect the rain erosion behavior of SCFS (more test data is needed).

5. For missile flights in natural rainfields equivalent to the artificial rainfield at Holloman Air Force Base, it is recommended that the impingement angle be controlled so that the normal component of the freestream velocity not exceed 500 m/sec (1640 ft/sec) on an SCFS radome.

TABLE 1. SAMPLE PERFORMANCE

Test No.- Sample No.	Material	Density (g/cc)	Coating	Semivertex Angle (deg)	Maximum Depth of Penetration (mm)	Maximum Depth of Penetration Rate (mm/sec)	Pre-test Weight (g)	Weight Loss (g)	Average Depth of Penetration Rate (mm/sec)	S $V \sin \theta$ (m/sec)	Comments
1-1	SCFS'	1.90	None	15	0.191	0.51	-	Not Repr. Eros.	N/A	442	No longitudinal cracks. Base edge chipped 360°. Low density.
1-2	SCFS'	1.96	None	15	0.127	0.33	-				2 longitudinal cracks. Base edge chipped 350°.
1-3	SCFS'	1.96	SR80	15	0.127	0.33	-				3 longitudinal cracks. Base edge chipped 240°.
1-4	SCFS'	1.96	CR203	15	0.127	0.33	-				6 longitudinal cracks. Base edge chipped 180°.
1-5	SCFS'	1.96	None	15	0.127	0.33	-				3 longitudinal cracks. Base edge chipped 360°.
1-6	SCFS'	1.96	SR80	15	0.127	0.33	-				No longitudinal cracks. Base edge chipped 360°.
1-7	SCFS'	1.96	None	15	0.127	0.33	-				3 longitudinal cracks. Base edge chipped 270°.
2-1	SCFS'	1.95	CR203	15	-	-	120.885	-	-	433	Lost sample (large piece lost in rainfield).
2-2	SCFS'	1.96	None	15	0.127	0.19	149.915	0.659	0.09		Negligible erosion.
2-3	SCFS'	1.96	SR80	15	0.127	0.19	121.132	0.700	0.09		Negligible erosion.
2-4	SCFS'	1.97	1/2DC808	15	0.127	0.19	120.204	0.800	0.10		Negligible erosion.
2-5	Avcoat ⁺ 8027	1.2	None	15	2.400	3.65	79.292	14.114	3.17		70% to 80% of loss due to ablation.
2-6	SCFS'	1.88	None	15	0.279	0.42	146.460	18.350	2.61		Low density.
2-7	SCFS'	1.97	None	22.5	-	-	92.477	-	-	641	Lost sample after it was eroded badly in rainfield.
3-1	SCFS'	1.93	None	22.5	-	-	91.115	45.12	-	653	Rainfield failure (test 3) subjected some samples to excessive H ₂ O.
3-2	SCFS'	1.94	None	15	0.127	0.254	119.227	0.823	0.15	442	Severe erosion. None correlatable. Erosion correlates.

TABLE 1. (Continued)

Test No.- Sample No.	Material	Density (g/cc)	Coating	Semivertex Angle (deg)	Maximum Depth of Penetration (mm)	Maximum Depth of Penetration Rate (mm/sec)	Pre-test Weight (g)	Weight Loss (g)	Average Depth of Penetration Rate (mm/sec)	$V \sin \theta$ (m/sec)	Comments
3-3	SCFS ¹	1.97	None	22.5	-	-	-	N/A	-	-	Lost sample.
3-4	SCFS ¹	1.95	None	22.5	-	-	-	N/A	-	-	Lost sample.
3-5	SCFS ¹	1.95	None	15	-	-	-	N/A	-	-	Lost sample.
3-6	SCFS ¹	1.92	SR60	22.5	-	-	-	-	-	-	Lost sample.
3-7	Avcoat ¹ 8027	1.2	None	22.5	4.445	8.89	60.319	17.94	7.28	653	Approximately 70% of loss was due to ablation.
4-1	SCFS ³	1.94	None	22.5	2.210	6.35	92.584	N/A	N/A	653	2 longitudinal cracks. Severe chipping on one side at base. Repre- sentative erosion.
4-2	SCFS ³	1.96	None	22.5	N/A	N/A	-	N/A	-	-	Lost sample.
4-3	SCFS ³	1.98	None	22.5	-	-	-	N/A	-	-	Lost sample.
4-4	RSSN ⁴	2.87	None	22.5	-	-	-	N/A	-	-	Lost sample before entering rainfield.
4-5	Avcoat ¹ 8027	1.2	None	22.5	4.191	12.043	60.305	18.04	9.41	664	Approximately 70% of loss is attributed to ablation.
4-6	HPSN ⁴	3.12	None	22.5	0	-	-	-	-	-	No erosion.
4-7	Teflon ¹	2.2	None	22.5	4.064	11.678	97.335	14.964	4.79	664	Severe pitting. Some of loss due to ablation.
5-1	SCFS ¹	1.955	SR60	22.5	3.708	10.338	93.065	13.350	4.657	645	No visible cracks. Nonuniform but repre- sentative erosion.
5-2	SCFS ¹	1.956	None	19	0.964	2.413	120.274	0.804	0.233	550	No visible cracks. Nonuniform but repre- sentative erosion.
5-3	SCFS ¹	1.965	None	22.5	1.880	5.232	94.022	7.050	2.447	645	No visible cracks. Nonuniform but repre- sentative erosion.
5-4	SCFS ¹	1.958	None	19	1.372	3.810	120.824	0.341	0.088	550	2 circumferential and 3 longitudinal cracks not representative. Erosion away from cracks is representative.

TABLE 1. (Continued)

Test No.- Sample No.	Material	Density (g/cc)	Coating	Semivertex Angle (deg)	Maximum Depth of Penetration (mm)	Maximum Depth of Penetration Rate (mm/sec)	Pre-test Weight (g)	Weight Loss (g)	Average Depth of Penetration Rate (mm/sec)	$V \sin \theta$ (m/sec)	Comments
5-5	SCFS	1.958	Nona	22.5	3.046	6.464	82.370	6.219	2.165	645	No visible cracks. Non-uniform but representative erosion.
5-6	SCFS	1.954	SR60	19	1.651	4.597	121.434	10.138	N/A	550	1 circumferential and 4 longitudinal cracks not representative. Erosion away from cracks is representative.
5-7	Quartz-Polyimide	1.7	Epoxy	22.5	4.216	11.735	68.674	16.657	7.465	645	Random fiber quartz polyimide with 0.02 in. tape cover of same. Quartz was frayed, only 1 pit of 0.166 in. depth.
7-2	SCFS	1.96	None	22.5	2.74	7.74	80.57	14.9	4.66	659	Very severa erosion, cracks in sample.
8-1	SCFS	1.95	None	25	3.66	9.20	68.404	7.204	2.123	641	Medium erosion over 3/4 of sample, severe on 1/4.
6-2	SCFS	1.95	None	22.5	2.00	5.00	92.495	0.905	0.276	580	Minor erosion except for 2 cm ² area, 0.75 cm long crack.
6-3	SCFS	1.95	None	25	N/A	N/A	64.487	N/A	N/A	641	Severe erosion, data uncorrelatable, cracks in sample.
6-4	SCFS	1.96	None	19	0.50	1.25	113.490	0.234	0.064	494	Nagligible erosion over most of surface area.
6-5	SCFS	1.93	None	22.5	2.00	5.00	92.464	2.116	0.653	560	Minor erosion except for 3 to 4 cm ² area.
6-6	SCFS	1.93	None	25	3.30	6.25	65.461	10.151	3.023	641	Severe erosion over most of surface.
6-7	SCFS	1.95	None	22.5	2.20	5.50	83.172	1.738	0.530	560	Minor general erosion, severa for 4 cm ² area.
10-1	SCFS	1.94	None	27.5	1.00	2.09	92.985	1.645	0.475	566	Medium, near uniform erosion and pitting.
10-2	SCFS	1.97	None	30	1.76	3.72	102.952	5.675	1.504	637	Severa, near uniform erosion.
10-3	SCFS	1.97	None	27.5	1.40	2.92	94.657	3.207	0.912	588	Severe erosion area of 2 cm ² , medium elstwhere.

TABLE 1. (Concluded)

Test No.- Sample No.	Material	Density (g/cc)	Coating	Semivertex Angle (deg)	Maximum Depth of Penetration (mm)	Maximum Depth of Penetration Rate (mm/sec)	Pre-test Weight (g)	Weight Loss (g)	Average Depth of Penetration Rate (mm/sec)	$V \sin \theta$ ⁵ (m/sec)	Comments
10-4	SCFS	1.97	None	30	1.80	3.76	101.081	6.475	1.715	637	Severely eroded but uniform.
10-5	SCFS	1.97	None	27.5	1.65	3.44	94.256	2.207	0.626	568	Severe erosion for 3 cm ² area, medium elsewhere.
10-6	SCFS	1.95	None	30	2.74	5.72	101.086	6.280	1.661	637	Near uniform erosion, except more severe over 5 cm ² area.
10-7	SCFS	1.95	None	25	1.27	2.65	67.060	1.175	0.314	536	Minor surface pitting except two 1/4 cm ² areas. One 1.2 cm long crack at base.
11-1	Silica ⁸	1.56	None	25	N/A	N/A	69.21	36.255	N/A	606	Very severe erosion, unaccept- able candidate material.
11-2	SCFS	1.95	None	27.5	4.00	9.41	93.525	16.767	5.392	682	Very severe erosion over most of surface.
11-3	SCFS	1.95	None	25	2.00	4.71	64.48	1.325	0.400	606	Severe erosion over 1/4 of surface.
11-4	SCFS	1.93	None	25	2.15	5.06	86.86	3.802	1.159	606	Severe erosion over most of surface.
11-5	SCFS	1.96	None	27.5	4.06	9.55	94.41	16.757	4.790	662	Very severe erosion over most of of surface.
11-6	SCFS	1.93	None	25	2.30	5.41	86.22	1.270	0.387	606	Severe erosion over 3/4 of surface.
11-7	SCFS	1.95	None	22.5	1.50	3.53	92.83	1.087	0.375	548	Minor erosion except for 3 pits, largest area of 1.5 cm ² .

Notes:

1. Sample manufactured by US Army Missile Command (MICOM) R&D Laboratory.
2. Sample manufactured by MICOM R&D Laboratory and coated by ONERA.
3. Sample manufactured by Engineering Experiment Station (EES) of Georgia Tech.
4. Sample manufactured by Avco Corporation.
5. Average freestream velocity in rain.
6. Sample manufactured by Army Mechanics and Materials Research Center.
7. Sample manufactured by Texas Instruments Corporation.
8. Silica-filled, filament-wound silica.

TABLE 2. TEST ENVIRONMENT

Test No.	Date of Test	Holloman Test No.	Hour of Test (MDT)	Ambient Temperature (K)	Barometric Pressure (KPa)	Reinfield* Length (m)	Average Velocity In Rain (m/sec)	Maximum Velocity In Rain (m/sec)	Time In Rain (sec)
1	10-24-74	48R-A1	0518	283	88.99	610	1725	1762	0.372
2	4-23-75	48R-B1	0628	287	87.73	1100	1676	1762	0.657
3	6-18-75	48R-C1	0523	294	86.66	853	1707	1752	0.500
4	6-13-75	48R-C2A	0531	296	87.59	610	1737	1790	0.348
5	11-5-75	48R-C3A	0517	279	88.99	610	1686	1746	0.359
7	9-2-76	52R-A2	0500	292	87.33	610	1727	1753	0.353
8	11-19-76	52R-B2	1812	287	87.18	610	1524	1561	0.400
10	6-30-77	52R-C1	0500	294	87.06	610	1272	1303	0.479
11	9-20-77	52R-D1	0450	295	87.13	610	1433	1503	0.425

*Reinfield description: Mean Standard Deviation

Rain rate (mm/hr) 67 27.4

Mass median drop diameter (mm) 1.37 0.28

Liquid water content (g/m³) 3.1 1.14

TABLE 3. SUMMARY OF BARE SCFS* SAMPLES TESTED IN ARTIFICIAL RAINFIELD

TEST NUMBER	MACH NO.	NUMBER OF SAMPLES SUCCESSFULLY TESTED					30
		15	19	22.5	25	27.5	
1-2-3-4-5-7	5.0	6	2	4			
8	4.5		1	3	2		
11	4.2			1	3	2	
10	3.7				1	3	3
TOTAL SAMPLES		6	3	8	6	5	3

*All samples listed had a density of $1.95 \pm 0.03 \text{ g/cm}^3$.

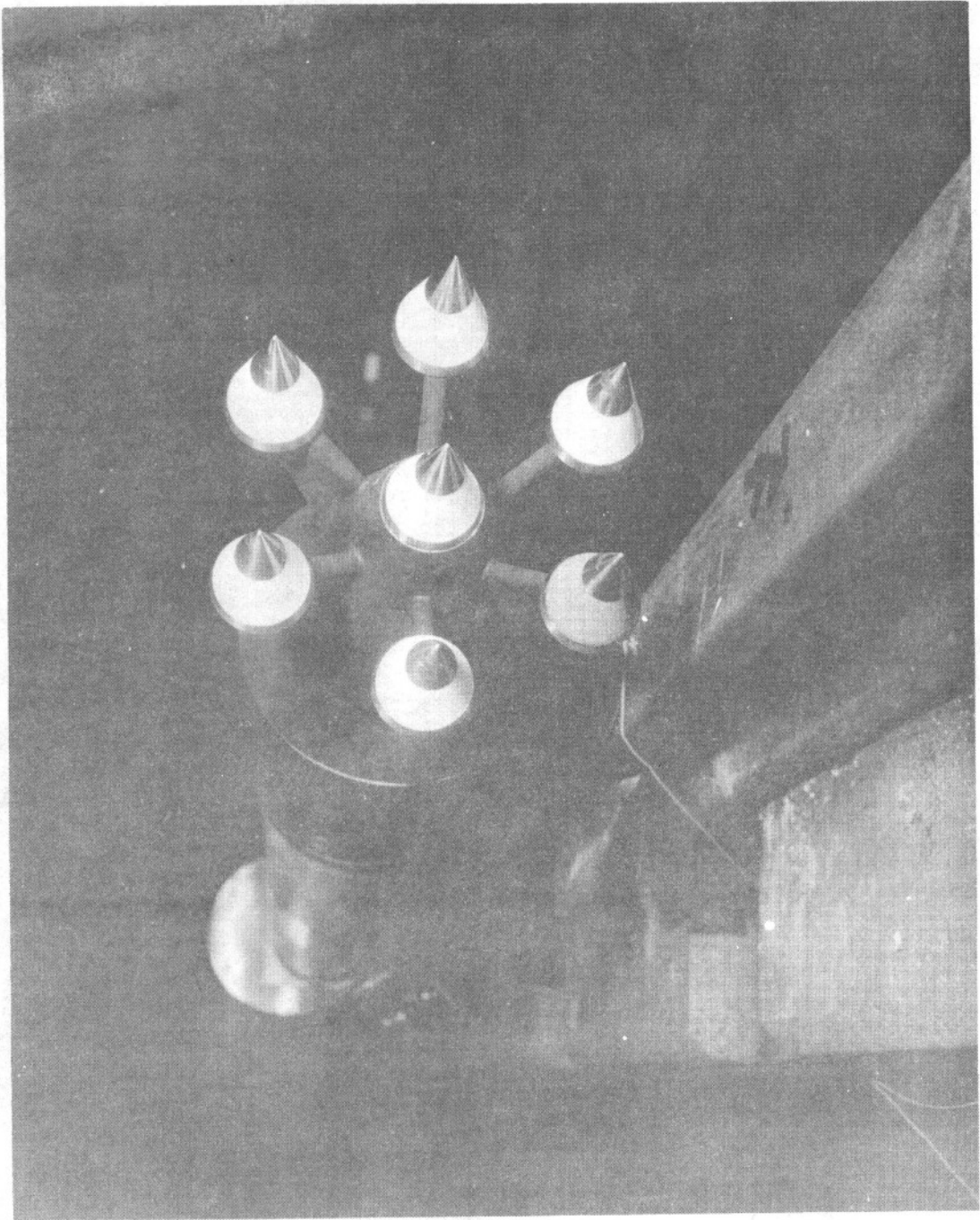


Figure 3. Samples assembled for test 1.



Figure 4. Post-test view of test vehicle and samples of test 1.

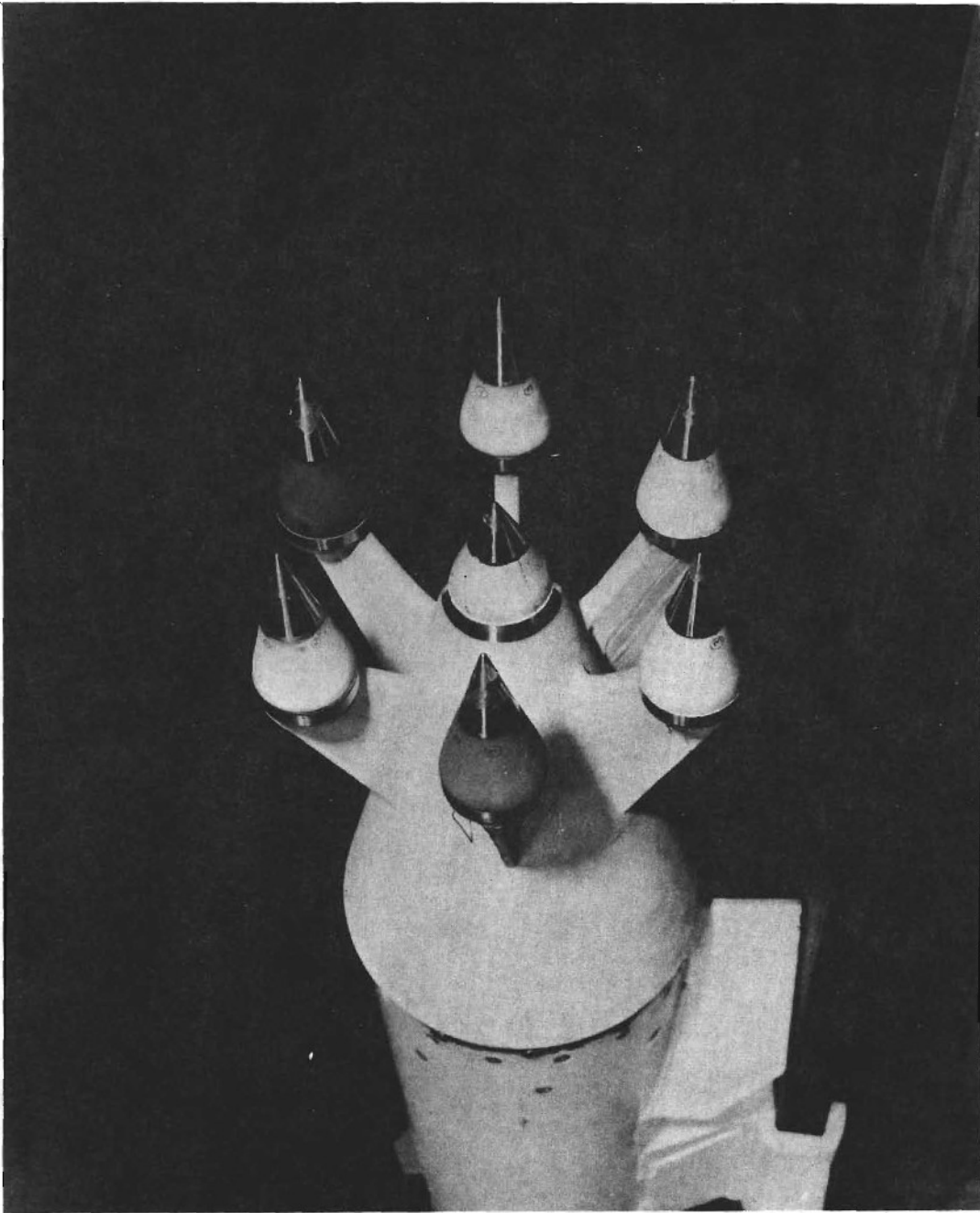


Figure 5. Samples assembled for test 2.

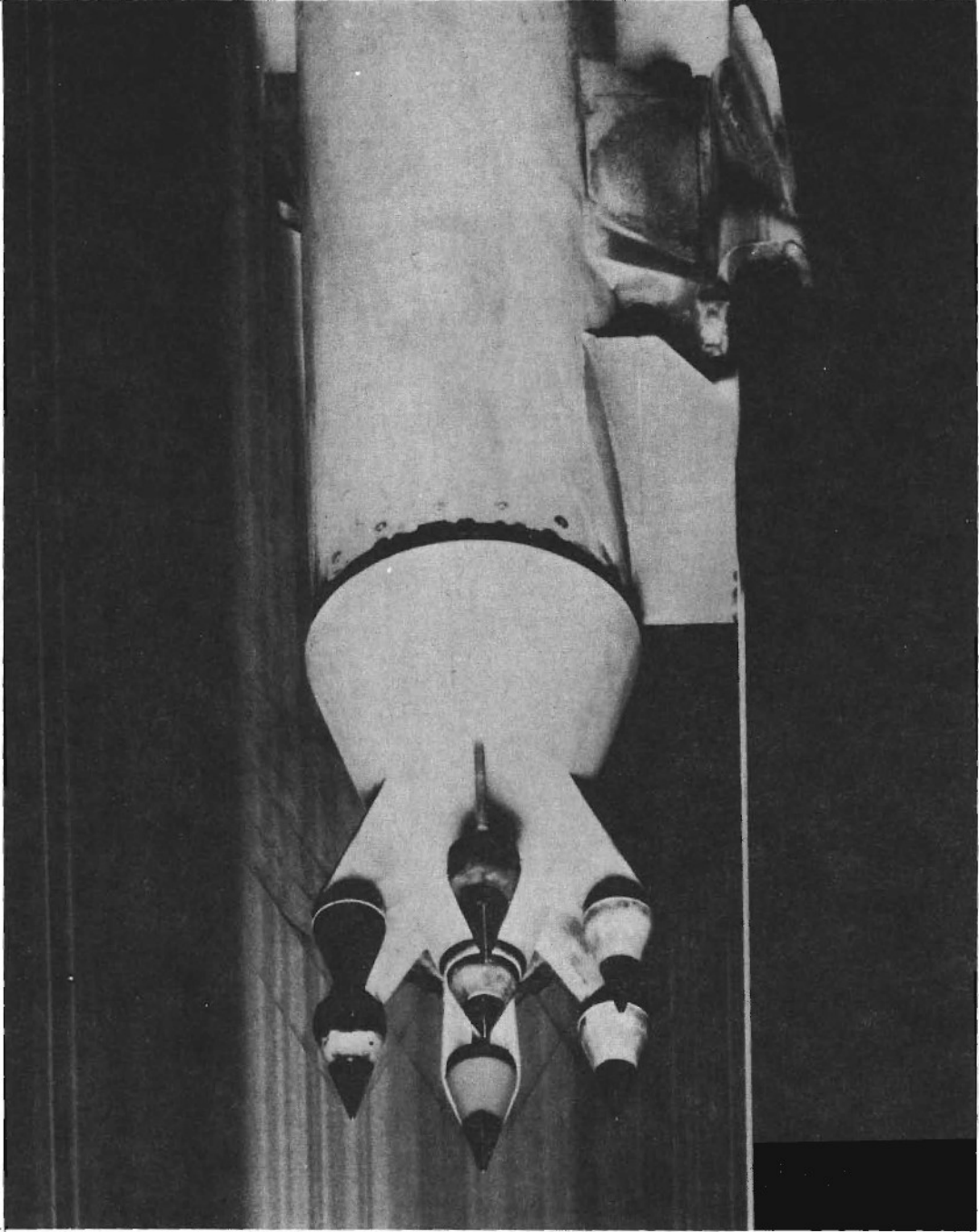


Figure 6. Mach 5 shocks on samples in test 2.

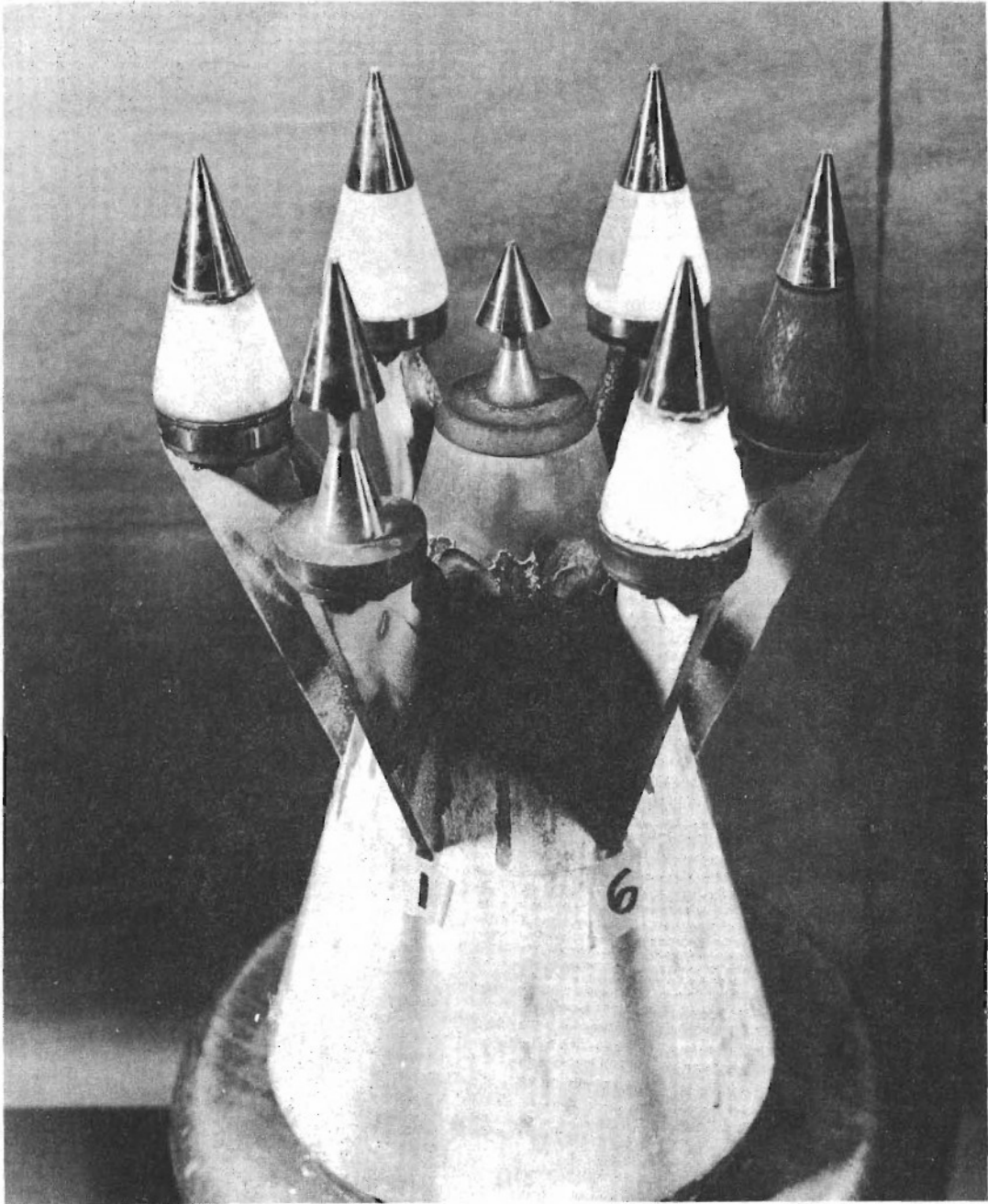


Figure 7. Test vehicle and samples after test 2.

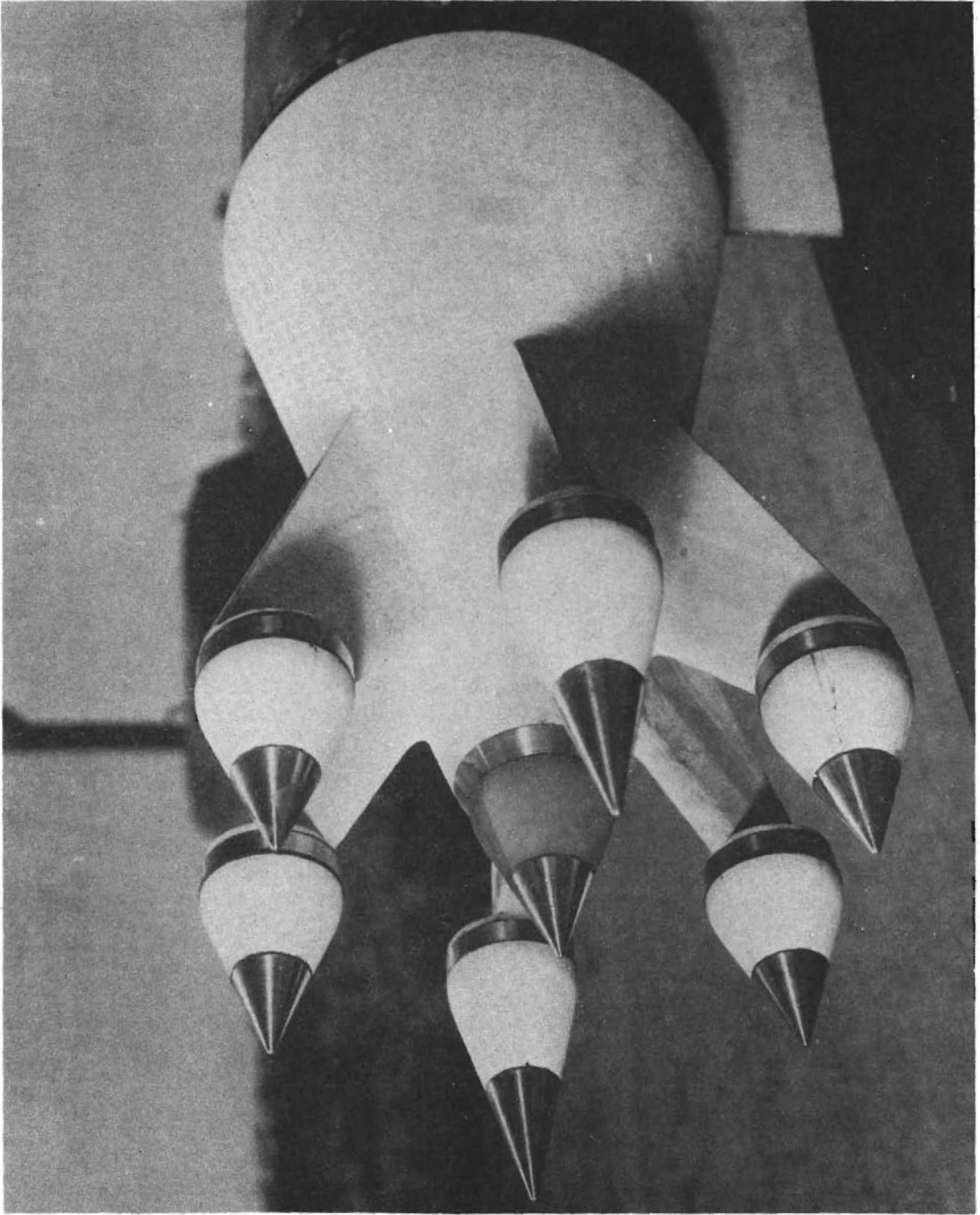


Figure 8. Samples assembled for test 3.



Figure 9. Test vehicle and samples after test 3.

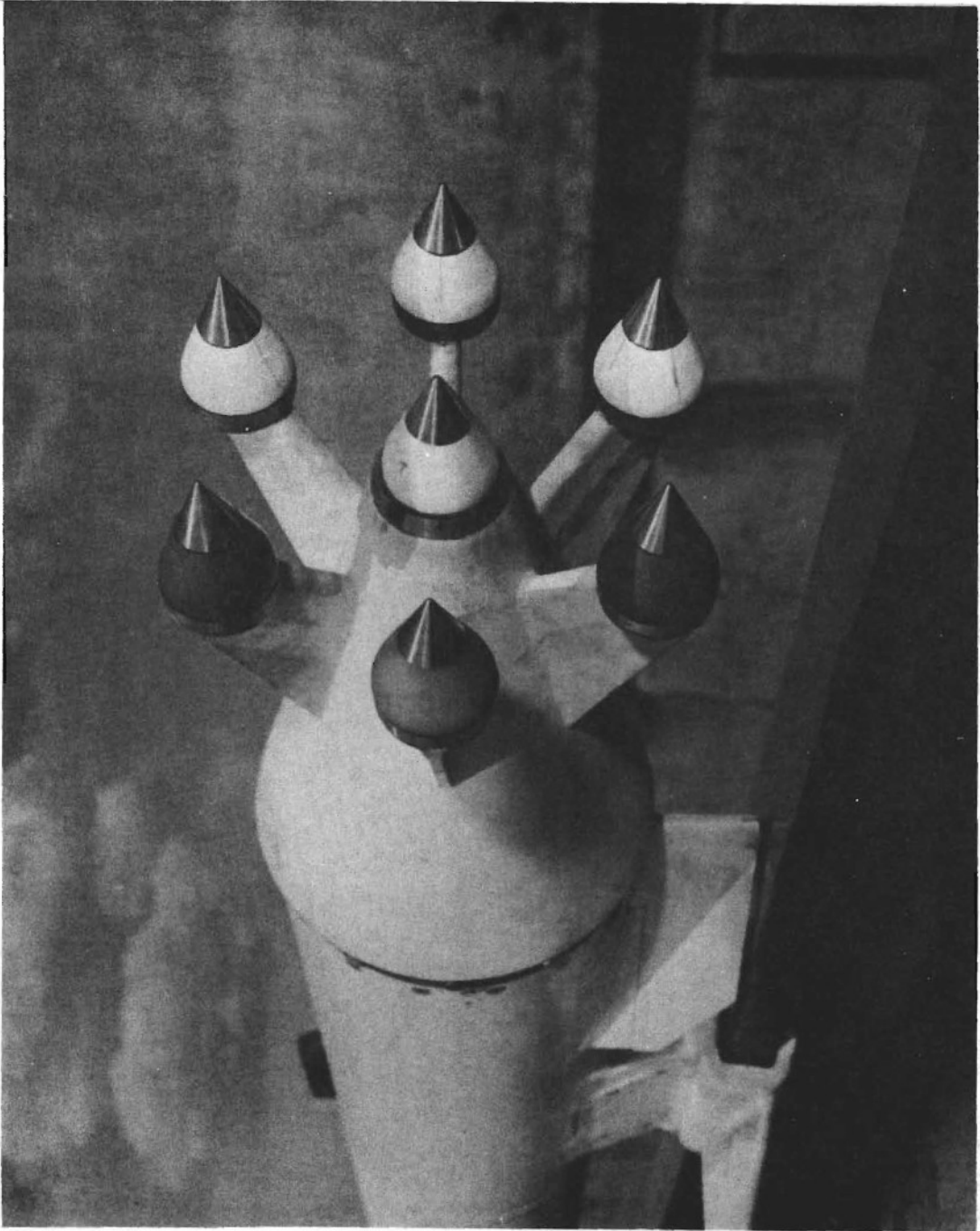


Figure 10. Samples assembled for test 4.

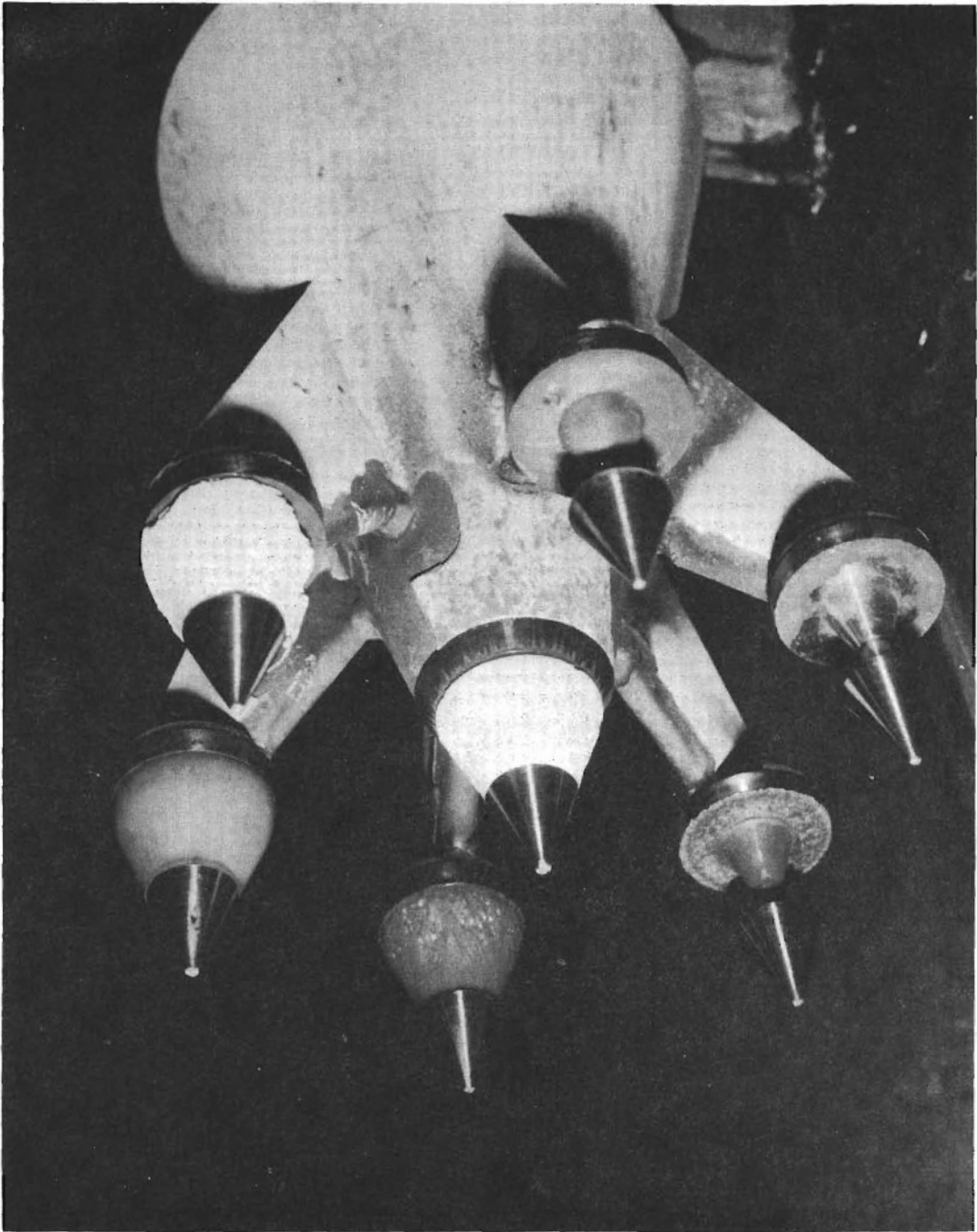


Figure 11. Test vehicle and samples after test 4.

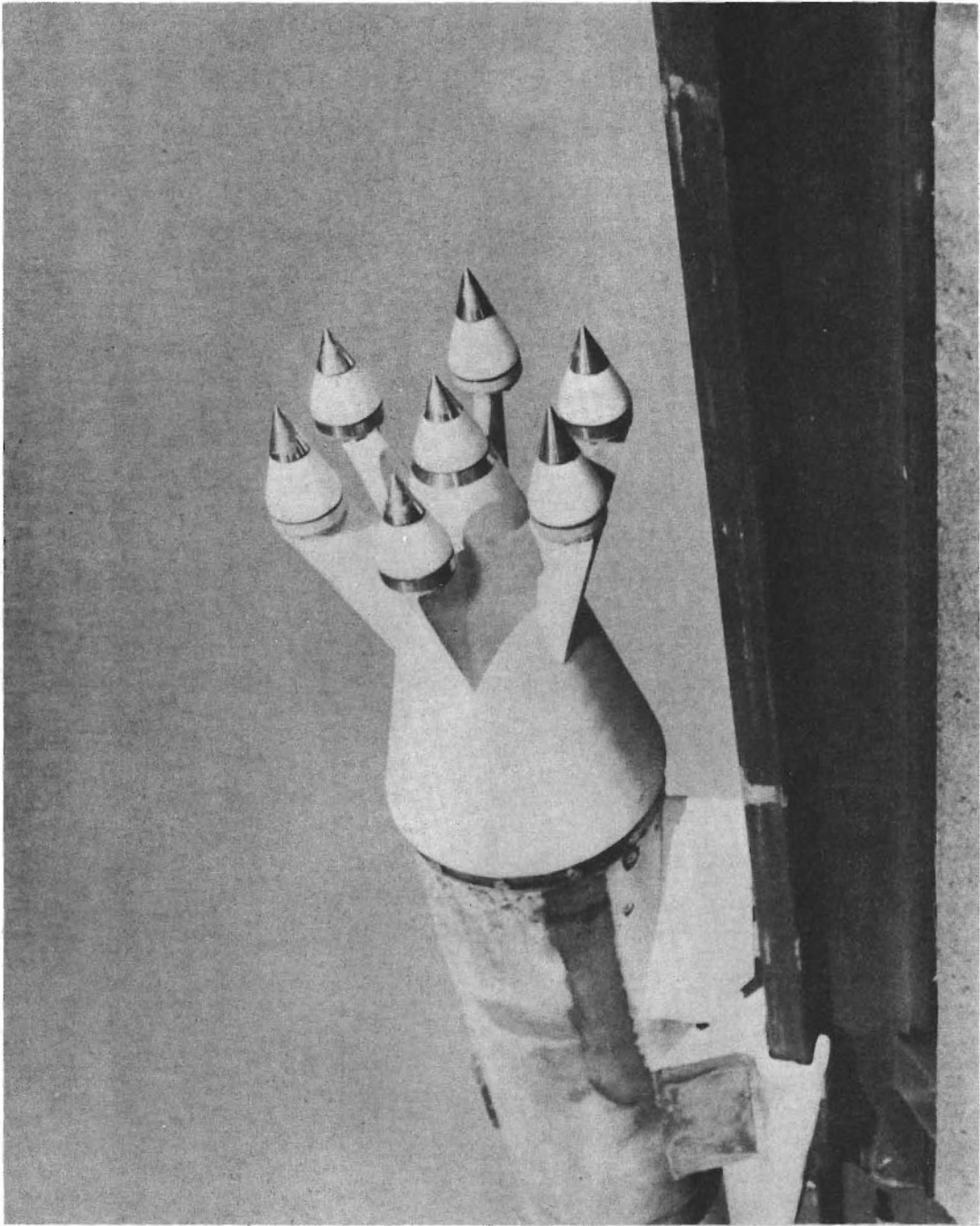


Figure 12. Samples assembled for test 5.

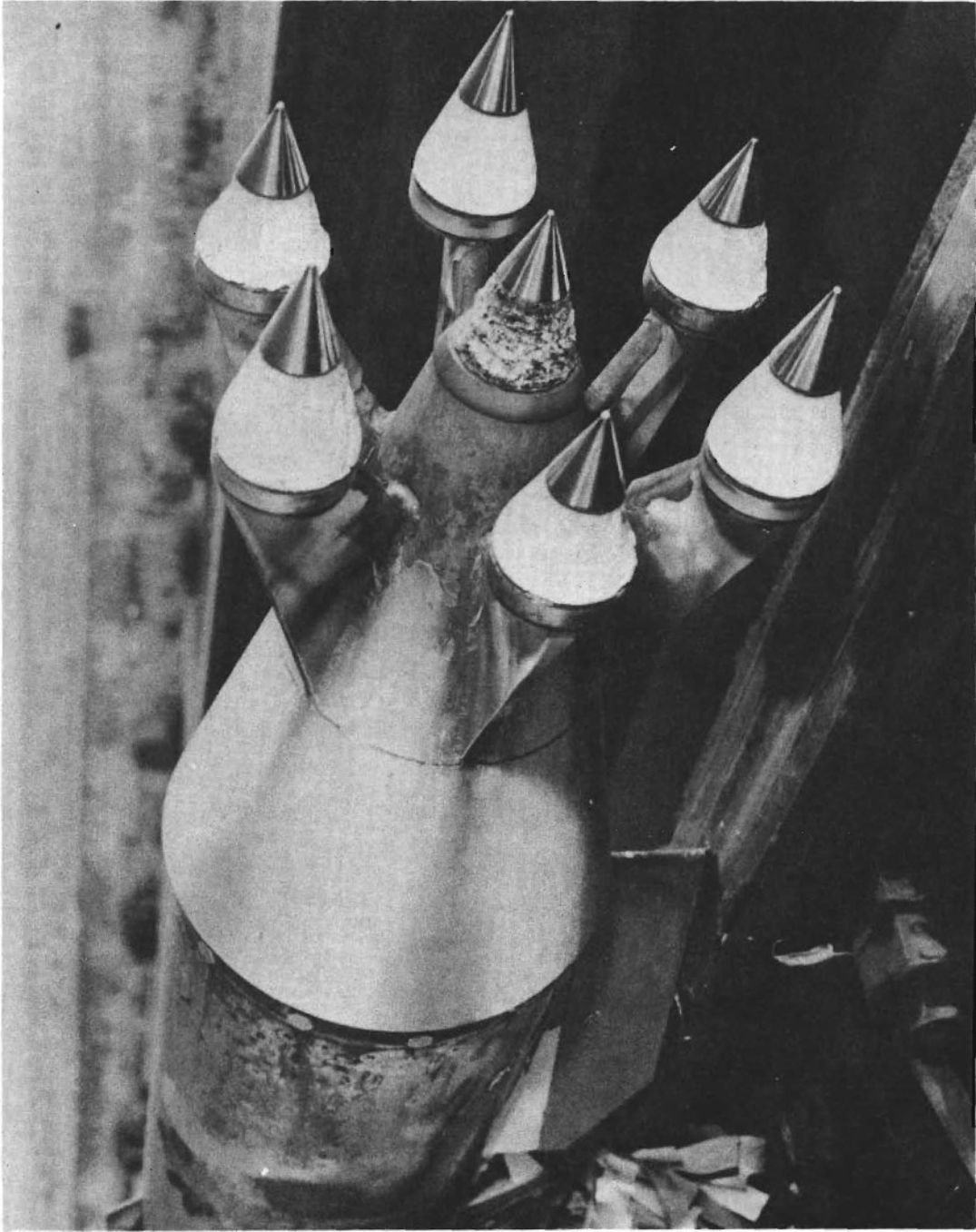


Figure 13. Test vehicle and samples after test 5.

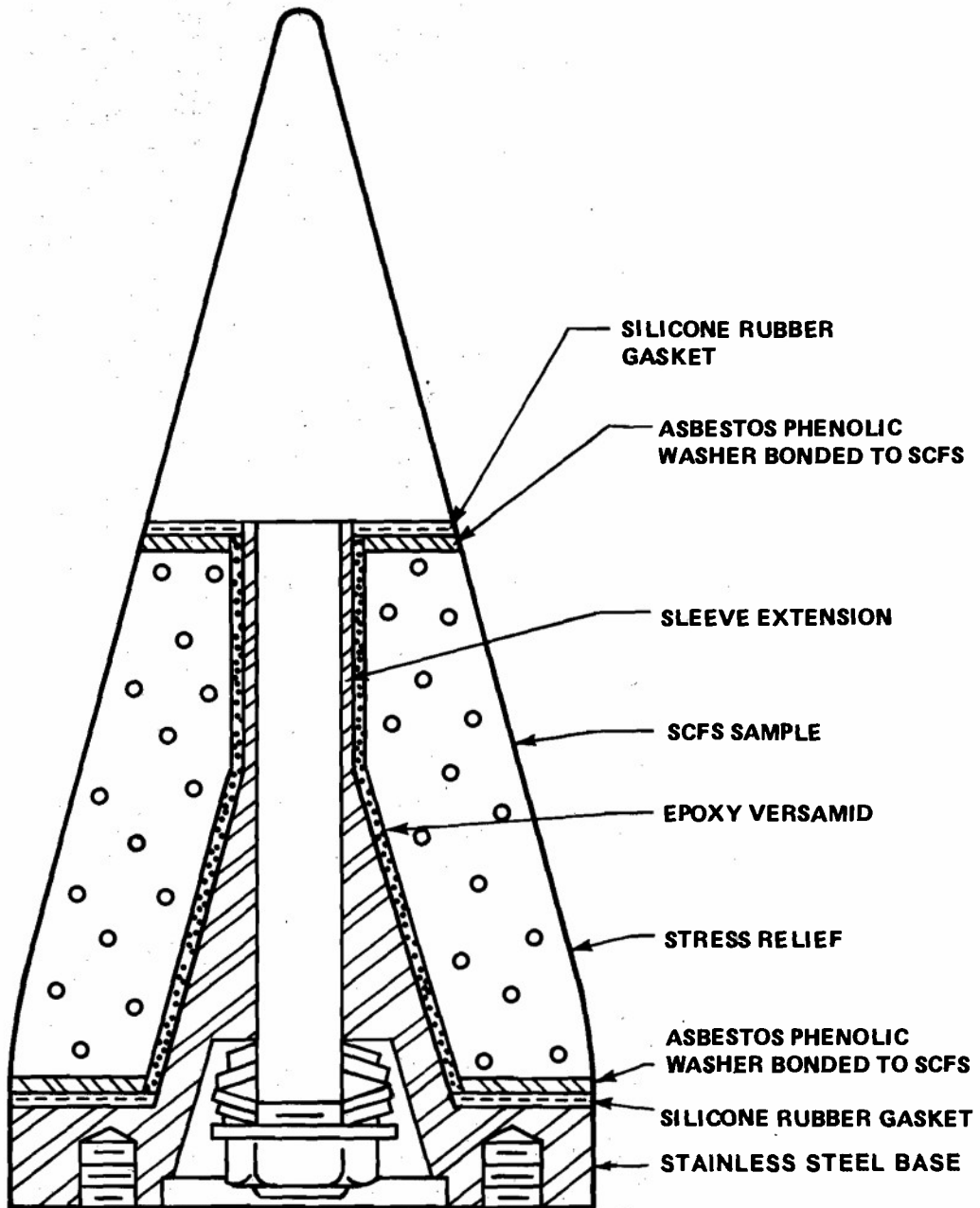


Figure 14. Modifications to sample subassembly for test 5 and subsequent tests.

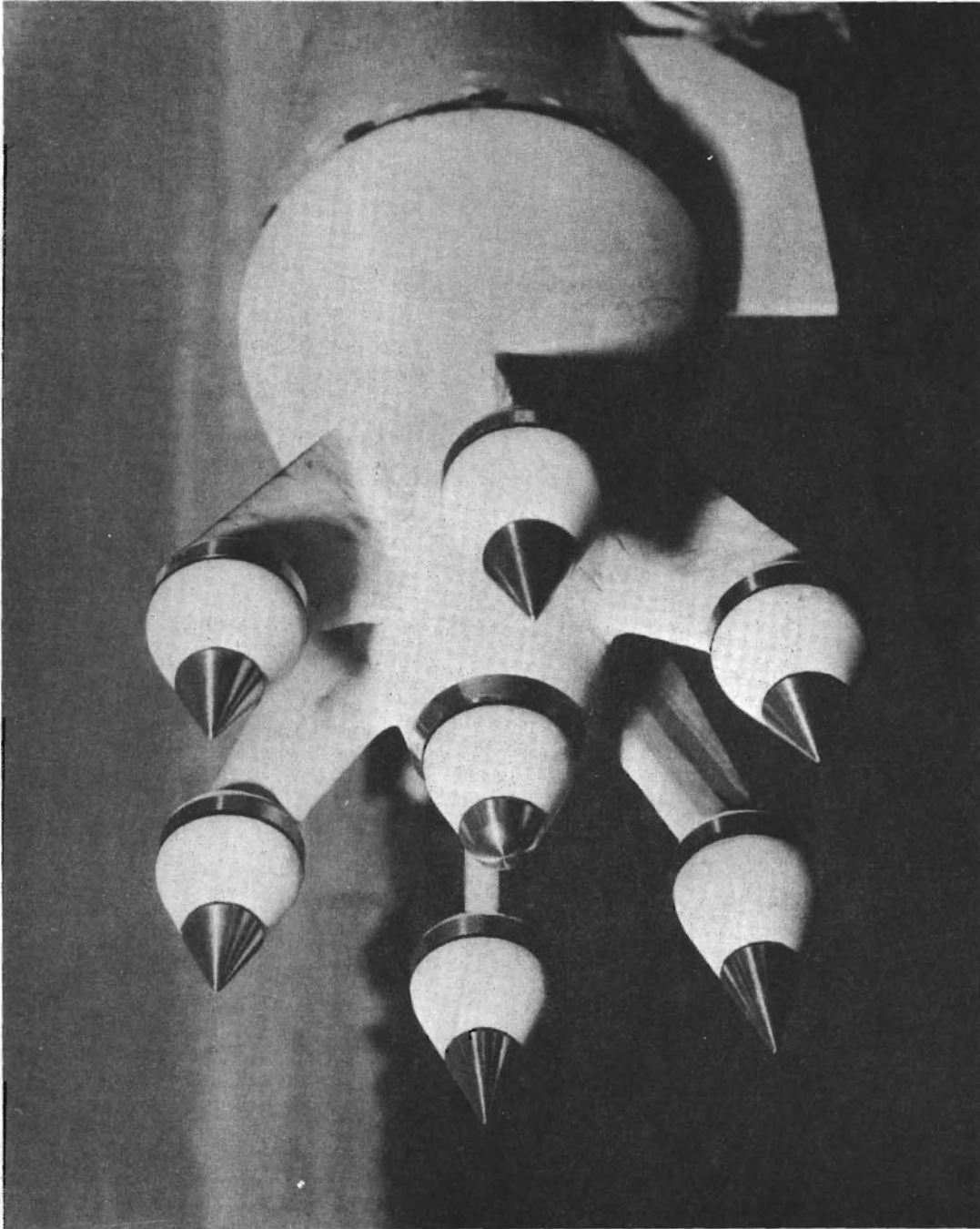


Figure 15. Samples assembled for test 8.

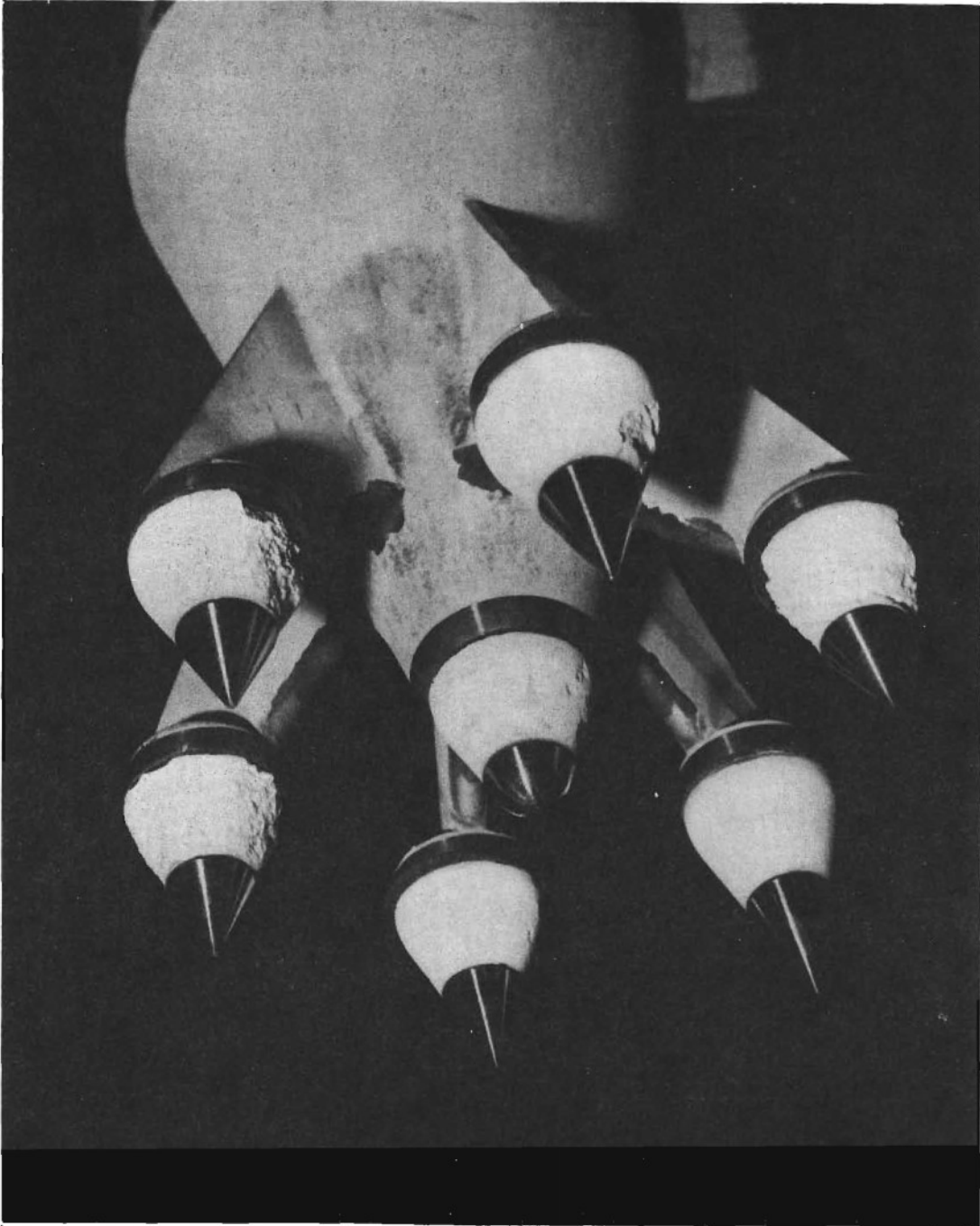


Figure 16. Test vehicle and samples after test 8.

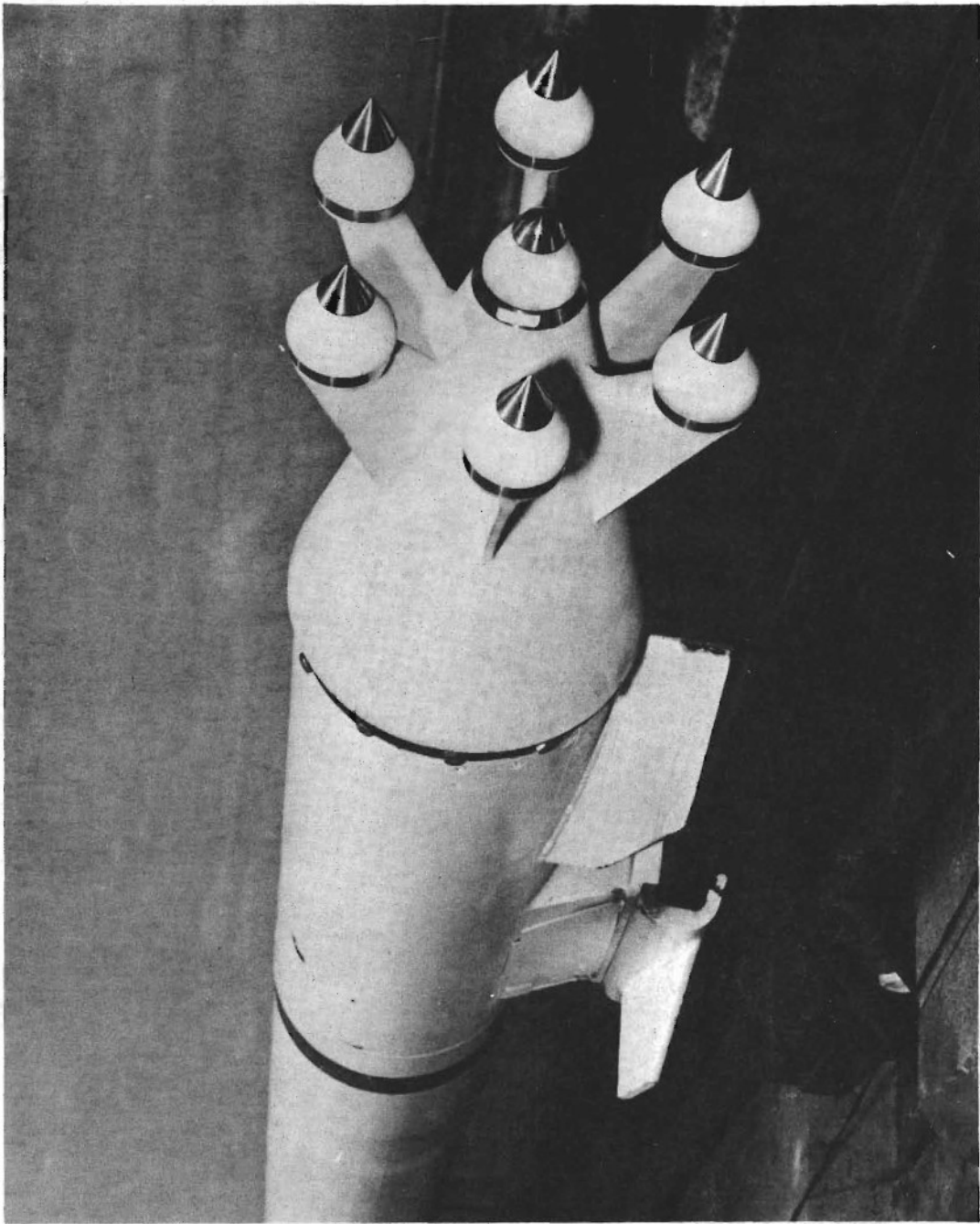


Figure 17. Samples assembled for test 10.

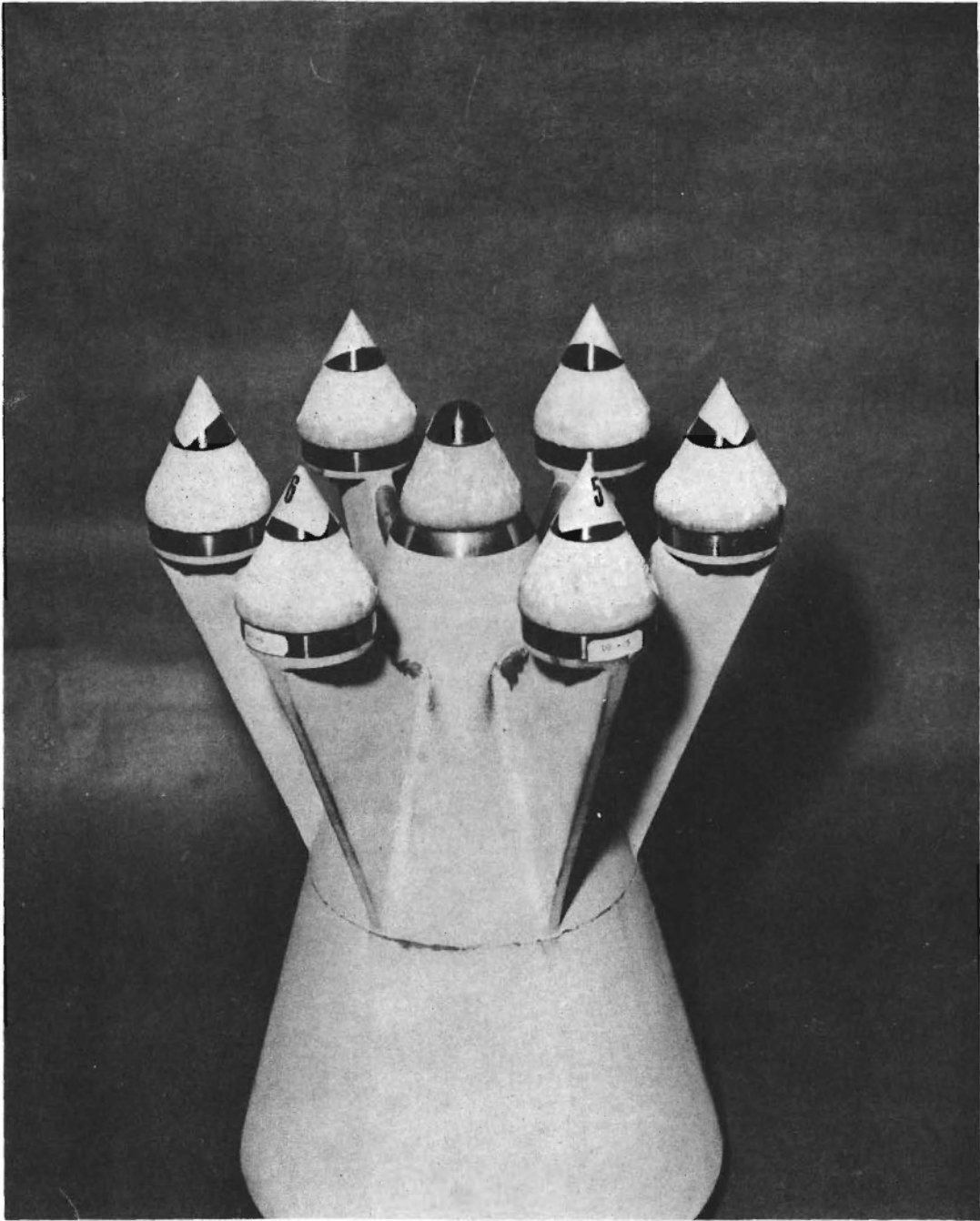


Figure 18. Test vehicle and samples after test 10.

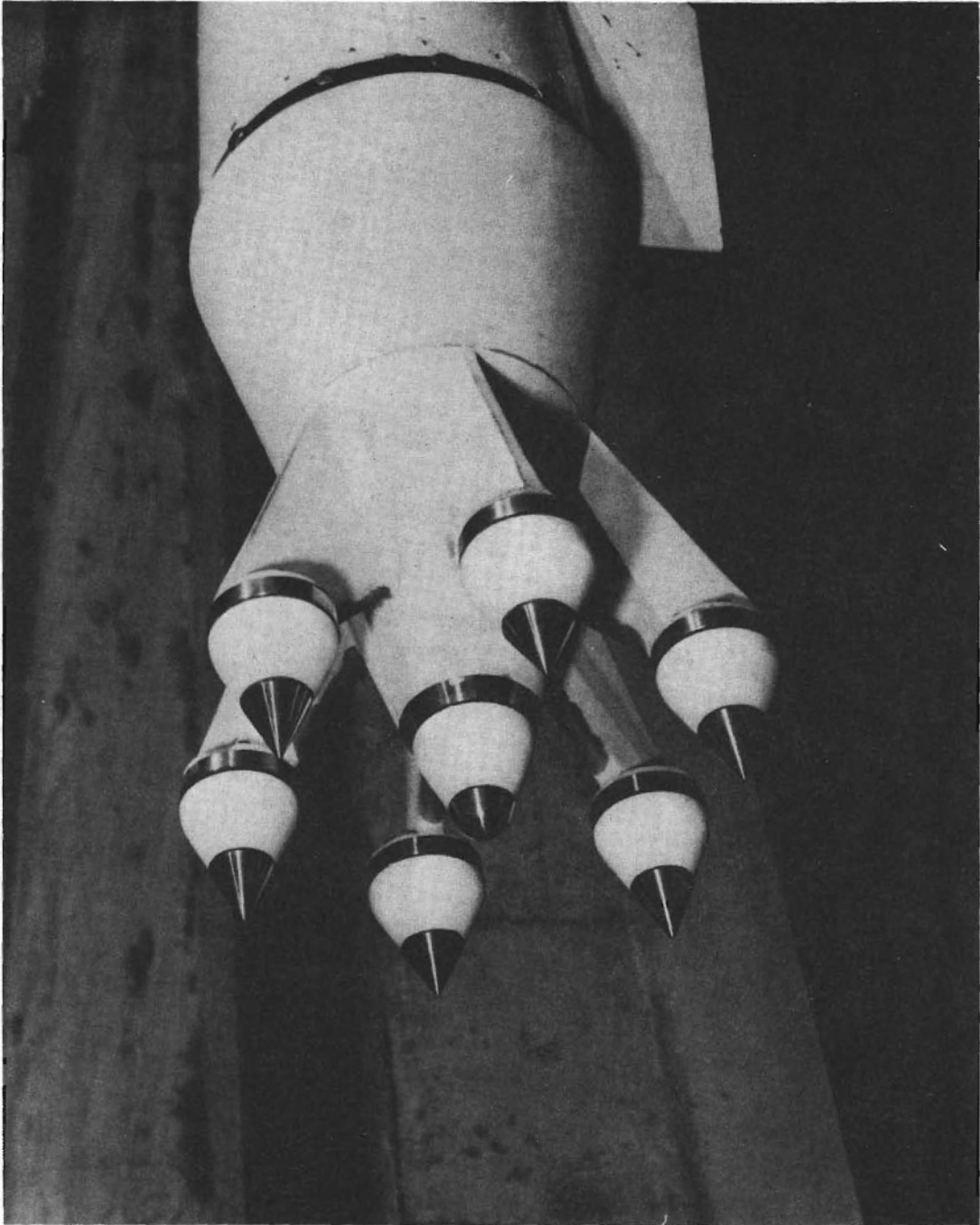


Figure 19. Samples assembled for test 11.

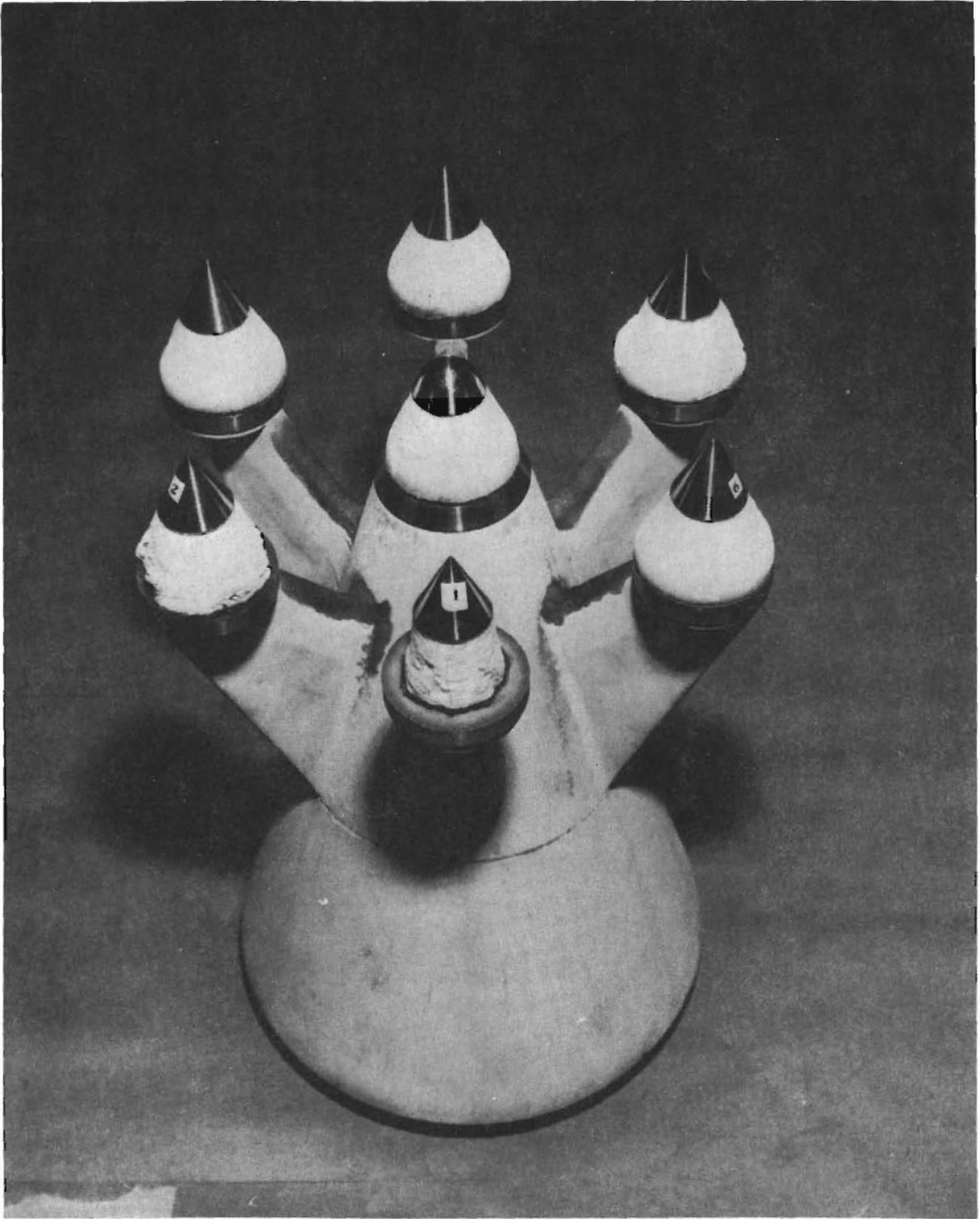


Figure 20. Test vehicle and samples after test 11.

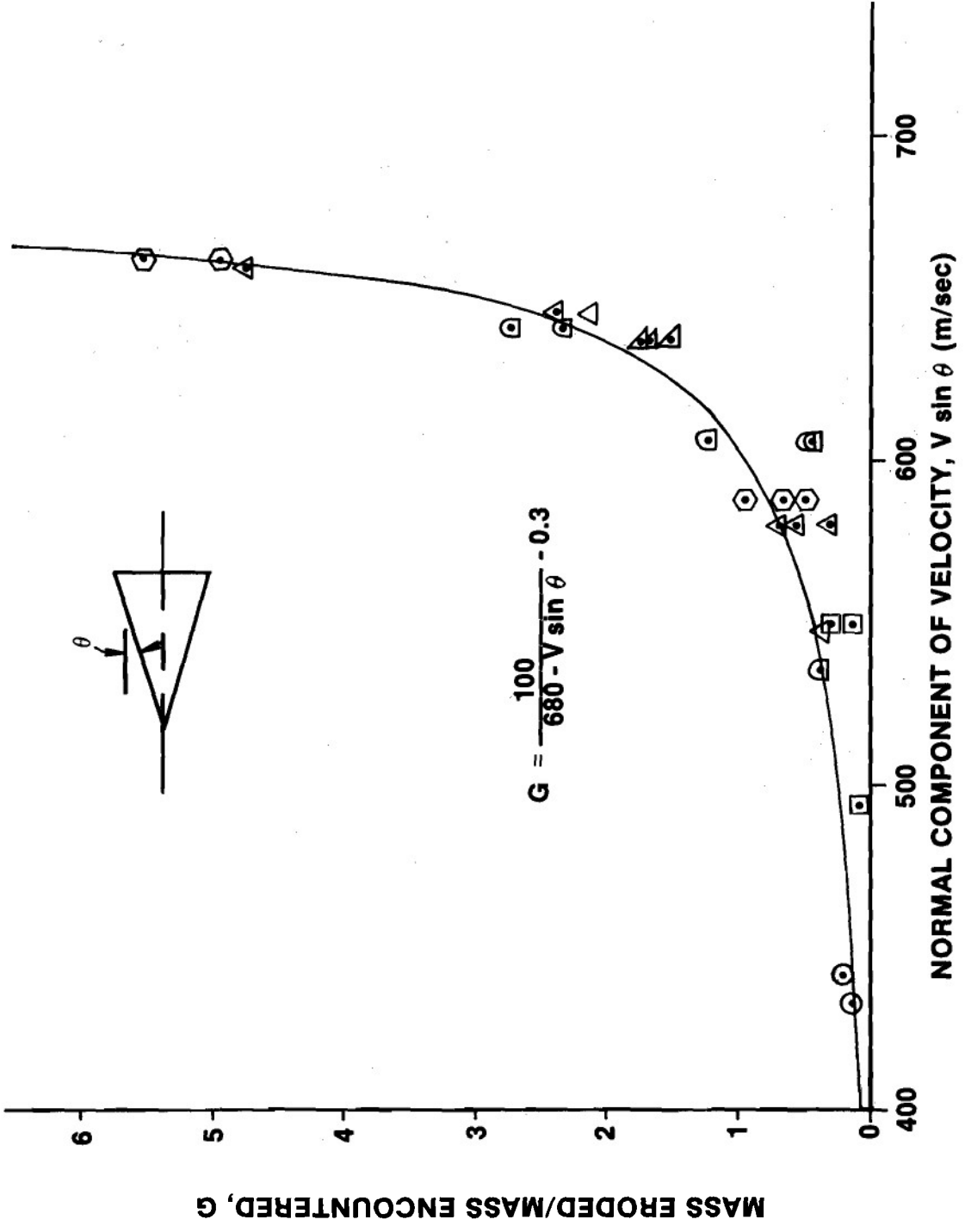


Figure 21. Rain erosion results for bare SCFS on supersonic sleds.

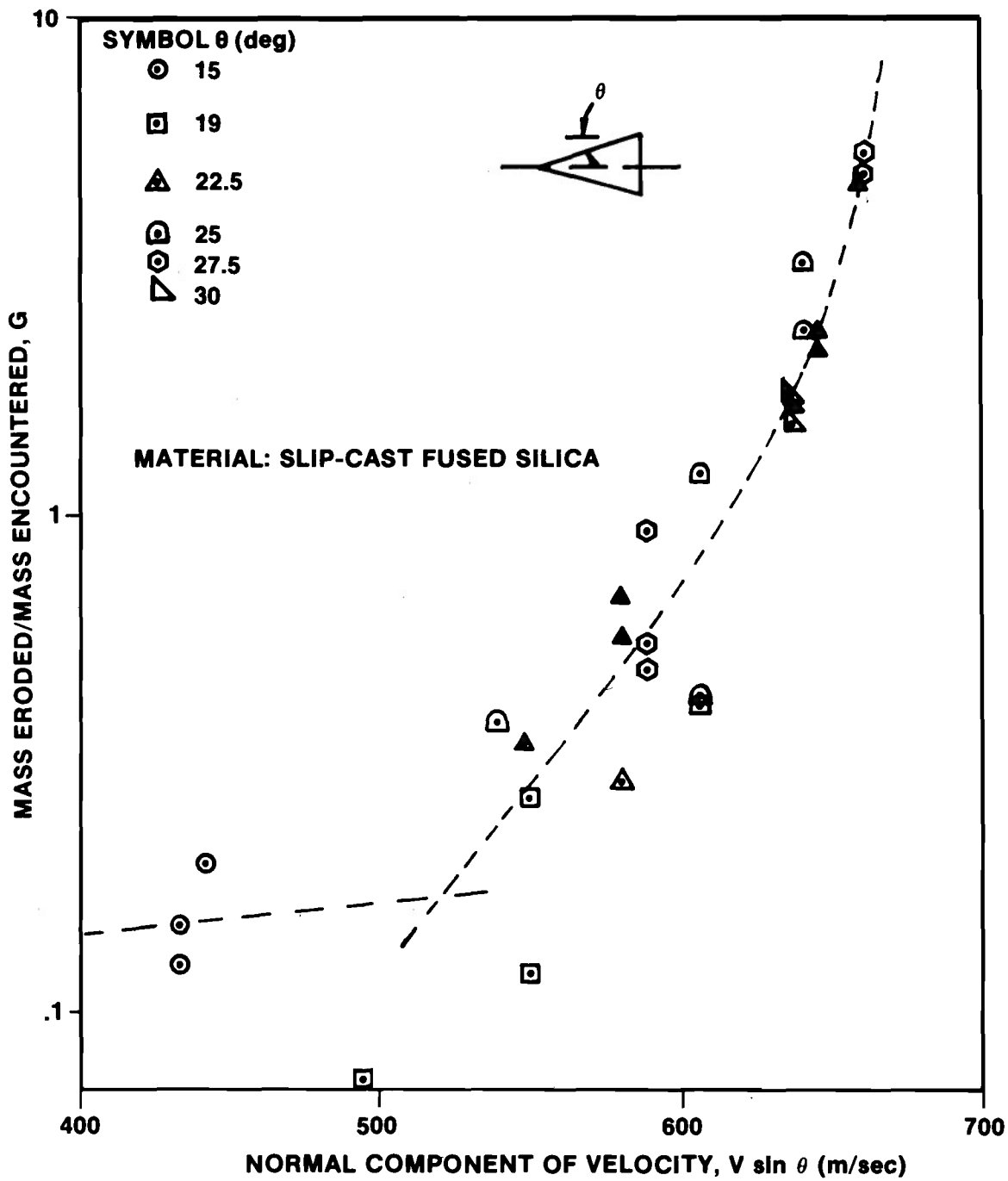


Figure 22. Rain erosion results for bare SCFS on supersonic sleds.

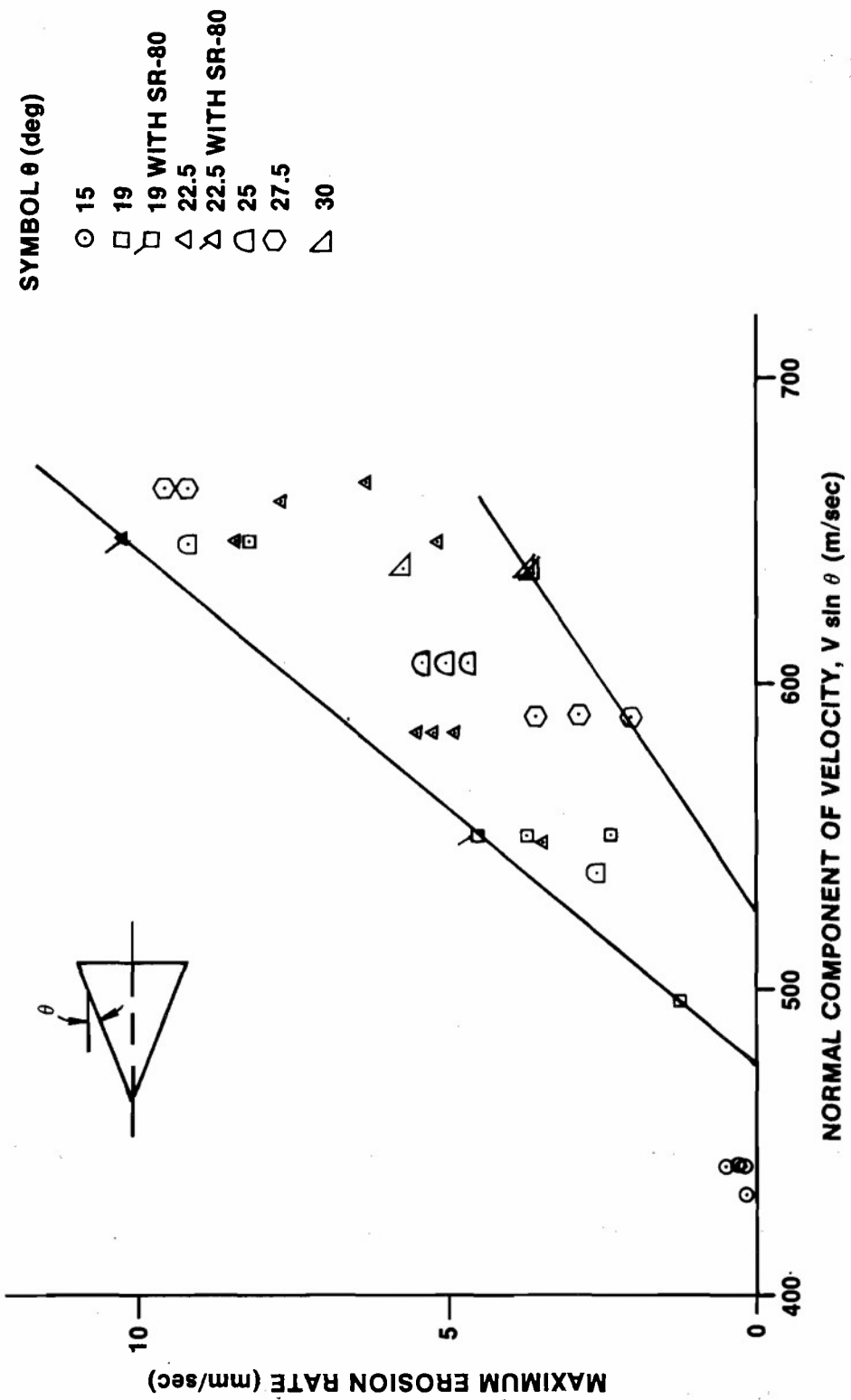


Figure 23. Measured maximum erosion rate of SCFS.

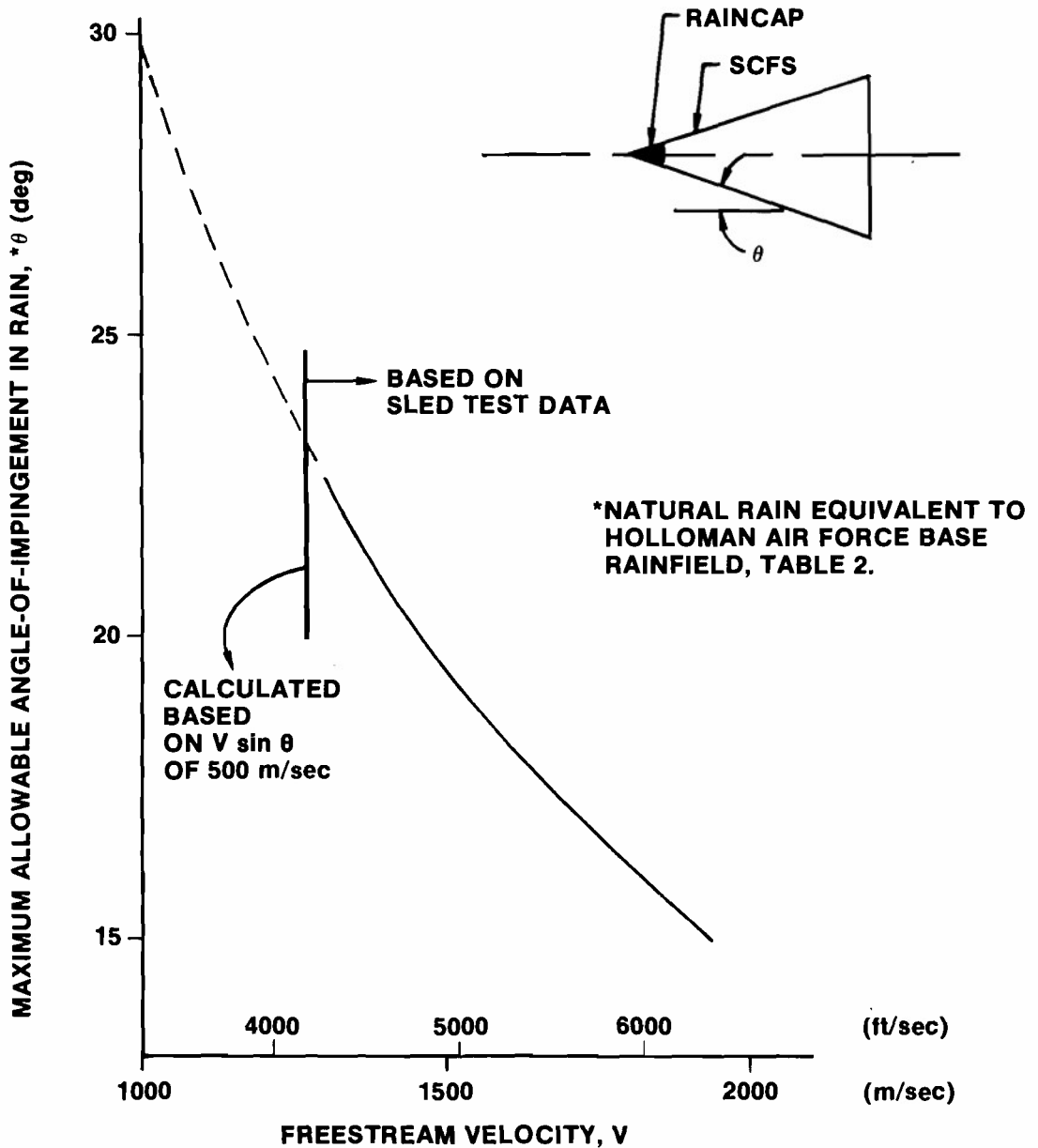


Figure 24. Allowable angle-of-impingement for SCFS

APPENDIX A TEST VEHICLE DESCRIPTION

The test vehicle was designed to carry a maximum number of samples consistent with achieving an average velocity of 5500 ft/sec through 2000 ft of the Holloman rainfield, to be compatible with the existing 9-in. monorail sled at the Holloman test track, to be structurally adequate for the environment, and to carry samples of the desired shape that would also minimize the risk of fracture due to stress risers related to size and shape. The resulting test vehicle and sample assembly are shown in *Figure A-1*. Analysis showed that seven samples of an adequate size could be carried efficiently, six of which could be supported by struts

welded into a 15 deg half-angle cone. The seventh could be carried at the front of the central cone.

The test vehicle was fabricated of 17-4 stainless steel except for the aft 7.5 in., the base section of the center cone, which was machined 4130 steel. The external surface of the test vehicle was coated with a high-temperature composite by Holloman test track personnel to minimize melting at regions of shock impingement. *Figure A-2* is a view of the test vehicle as fabricated before assembly and application of hardcoat insulation.

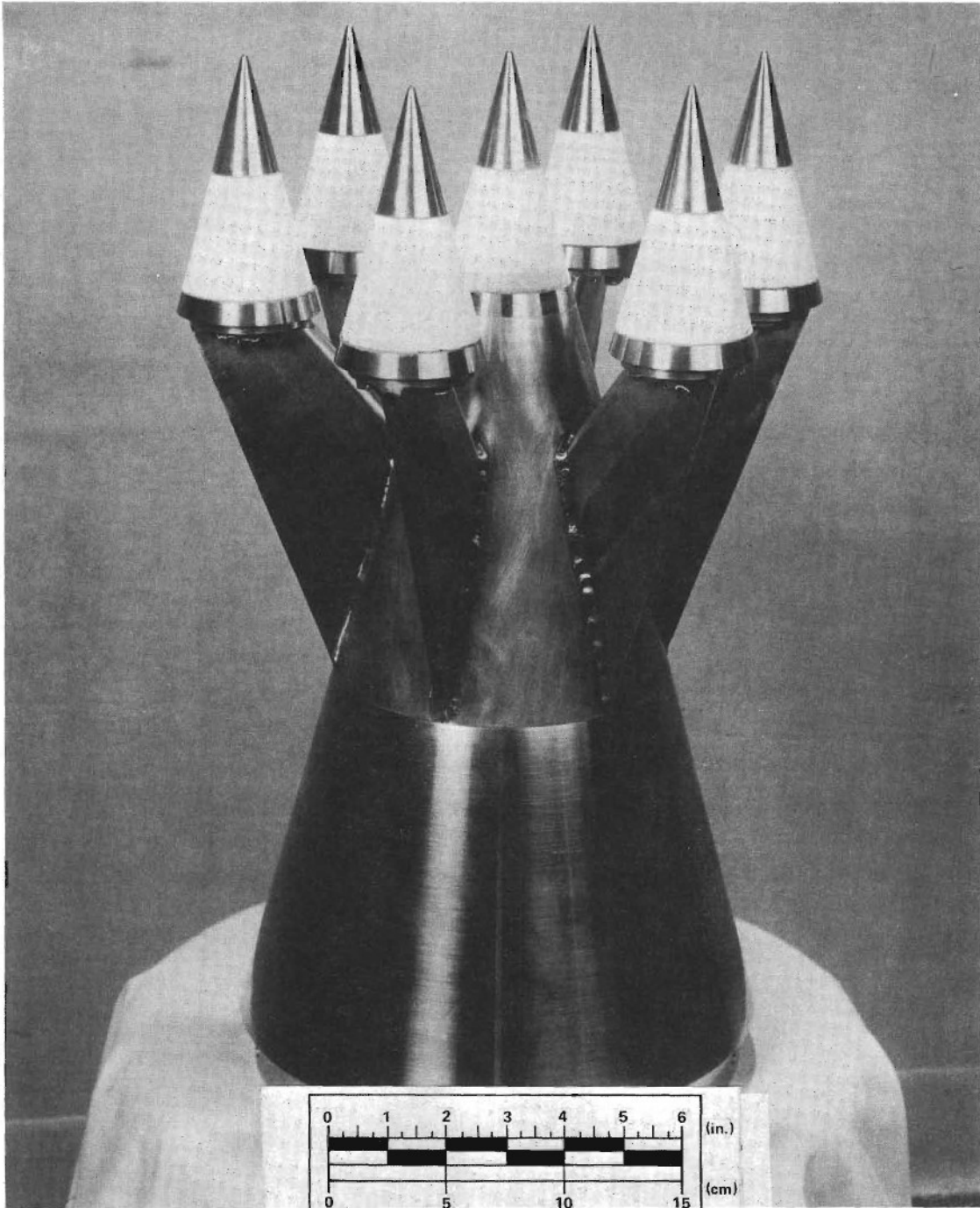


Figure A-1. Test vehicle assembly.

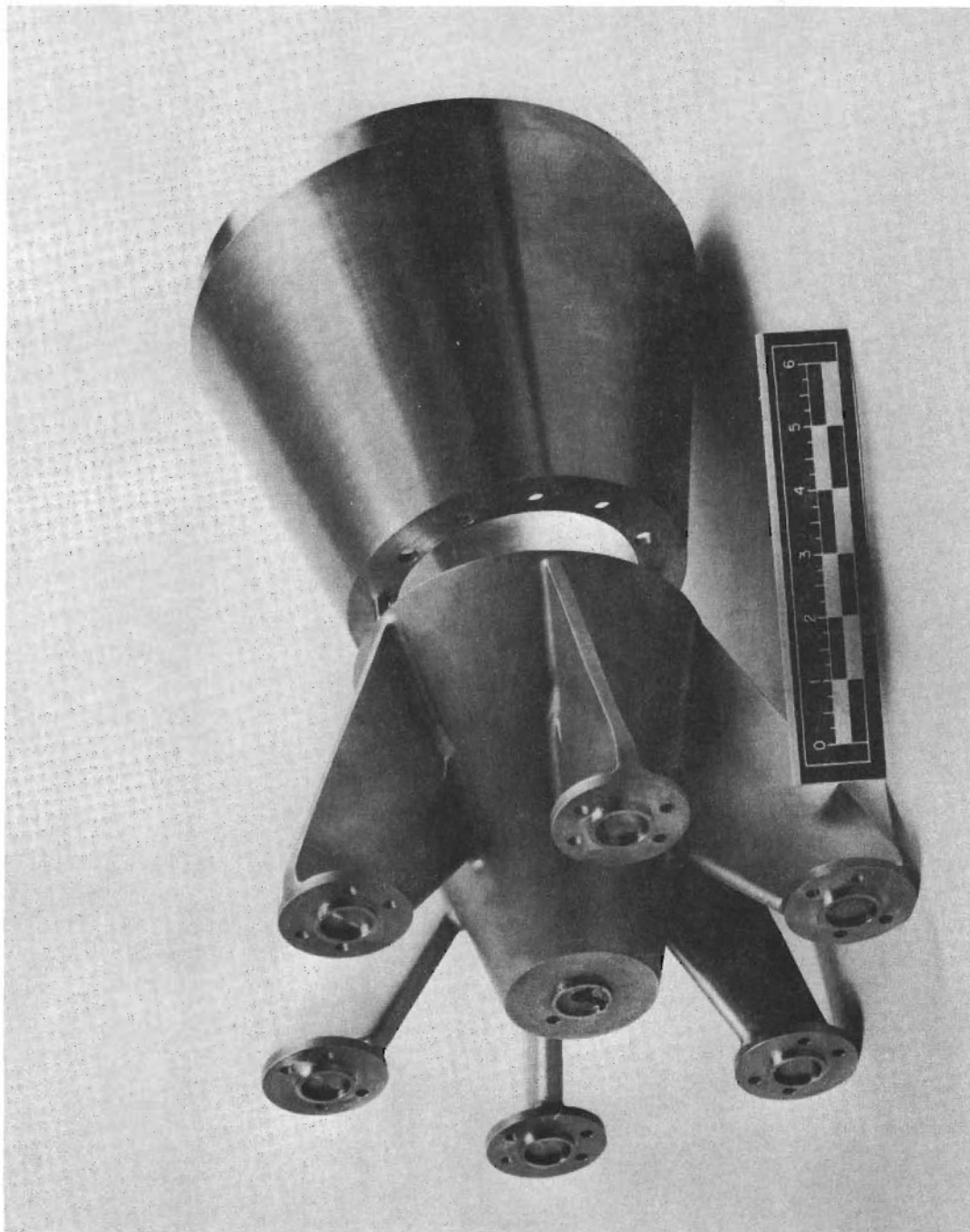


Figure A-2. Test vehicle.

APPENDIX B

TEST SPECIMEN SUBASSEMBLY DESIGN

The samples were designed to be mounted on the vehicle in a subassembly. Each cone frustum sample was assembled between a stainless steel tip and base before being mounted on the test vehicle. The initial sample subassembly design is shown in *Figure 2*.

The steel tip of the sample subassembly secures the cone frustum sample in the subassembly and serves as a rain cap representative of current design practice for SCFS radomes since SCFS is eroded severely by normal impact of rain at Mach 5.³

In the first test, gaskets of asbestos phenolic were used at each end of the samples to distribute loads uniformly (*Figure 2*).

A maximum preload on each sample of approximately 6900 kPa (1000 lb/sq in.) was applied to prevent loss of a sample if cracking occurred. The vibration loads expected to be induced by the track were applied to the vehicle and sample subassemblies, without damage, in a laboratory simulation prior to the first sled test. However, during the first sled test

severe chipping of the region near the sample base and longitudinal cracking occurred on most of the samples. There was evidence also, on the steel tip stud, that tip deflections had been severe. A typical result is shown in *Figure B-1*. These effects are attributed to a combination of sled vibration, rain impact and structural preload. To avoid these problems, modifications to the samples and to the mounting procedure were made. To eliminate chipping of the base edge of the samples a stress relief was provided to prevent raindrop impact on the base corner. To prevent longitudinal cracking of the samples the sample preload was reduced to one-half its value in the first test. The steel sleeve through which the tip stud passes was extended completely through the center of the sample to prevent tip vibration from imparting loads to the sample. Also, to reduce vibration and to distribute loads more uniformly to the samples, gaskets of silicone rubber were used instead of gaskets of asbestos phenolic at each end of each sample. Some of the samples provided by the High Temperature Materials Division of the Georgia Institute of Technology had invar washers bonded to each end of the samples. This concept was incorporated, but

asbestos phenolic was substituted for invar because of lower cost. As an additional aid in reducing the effects of sled vibration, epoxy versamid was used between the sample and sleeve. These modifications

were successful and led to the final design and mounting arrangement shown in *Figure 14* which has been completely successful in eliminating failures due to spurious causes.

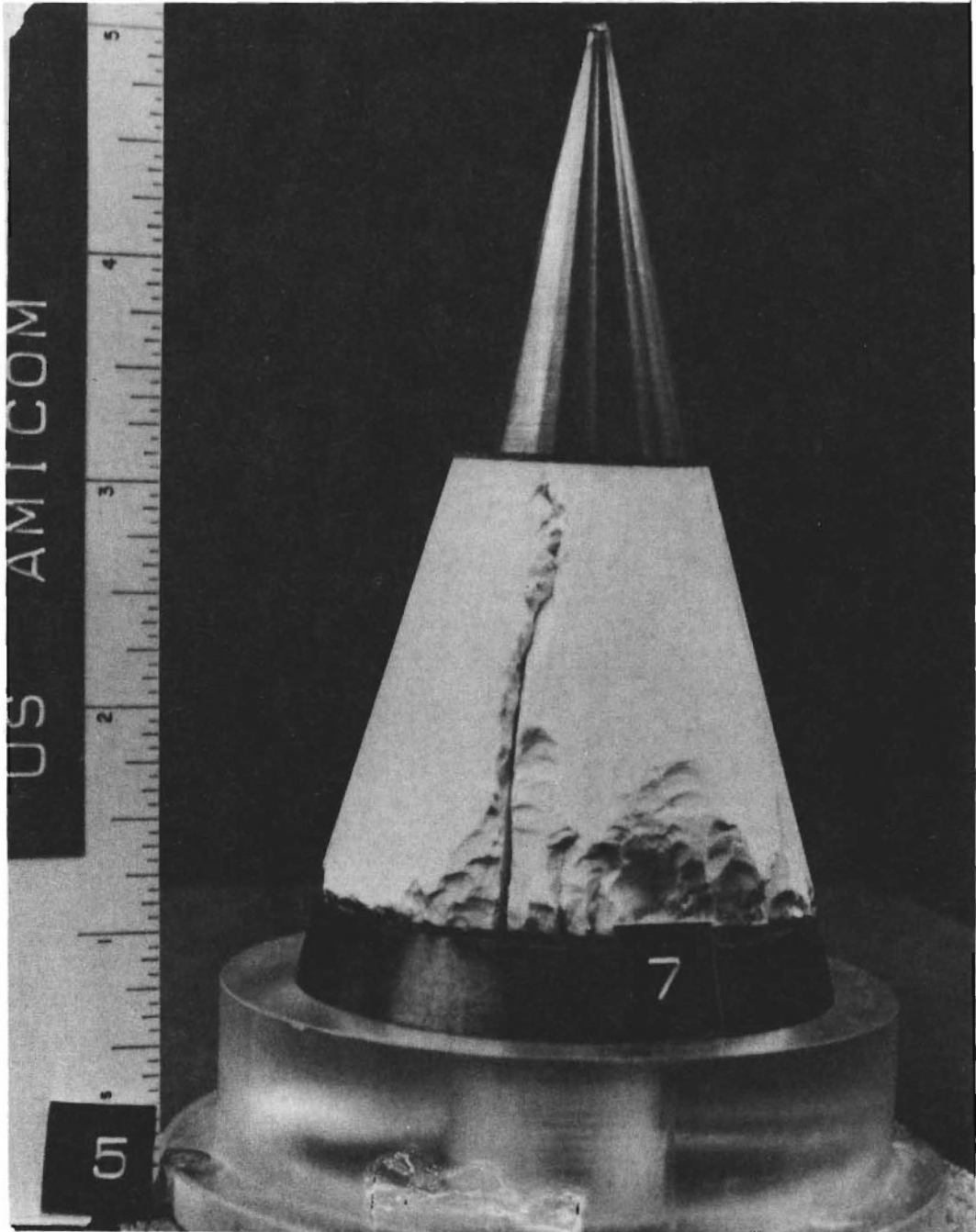
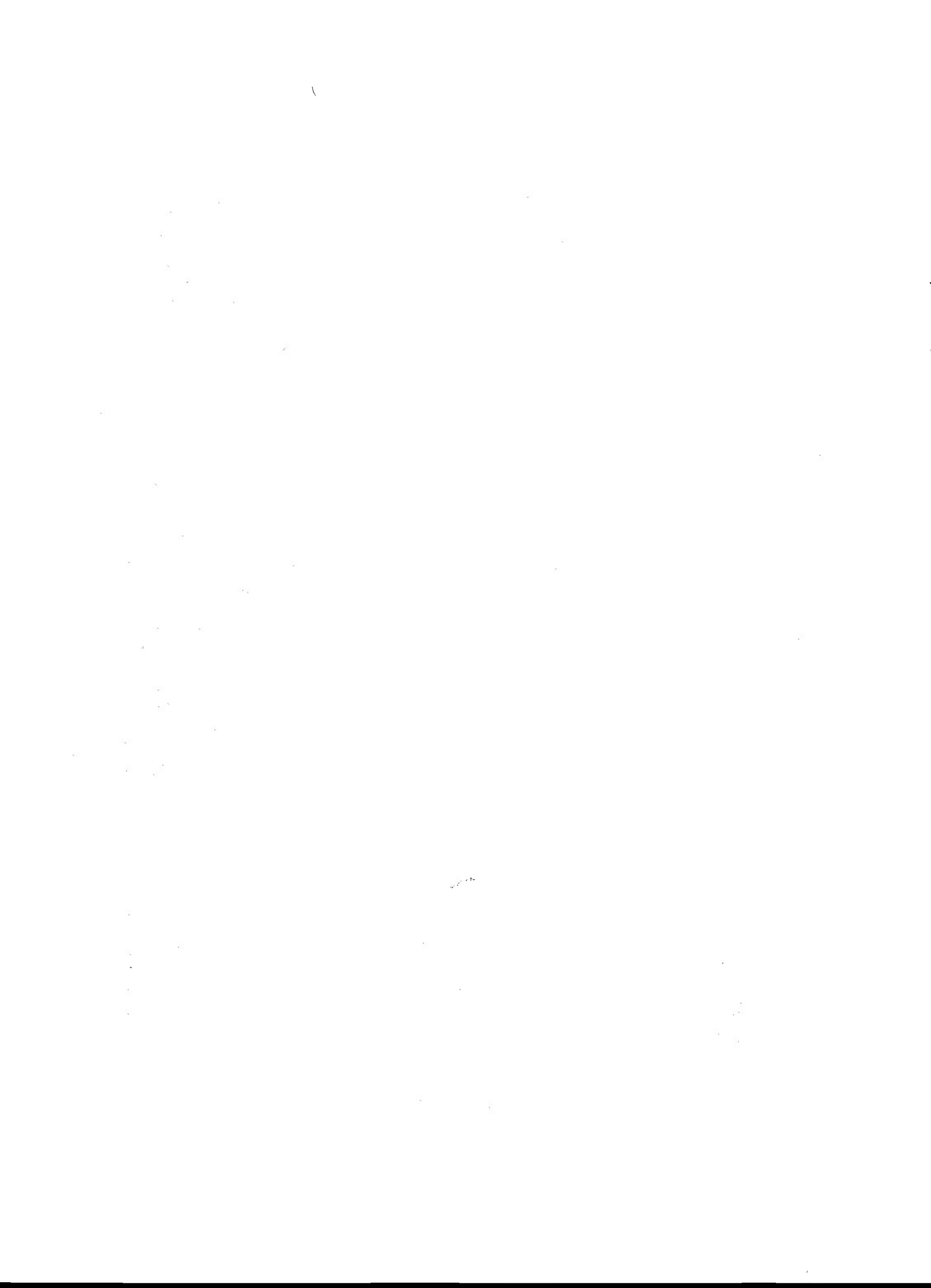


Figure B-1. Typical result from first test.



APPENDIX C TEST FACILITY

1. TEST TRACK

The test track at Holloman Air Force Base⁸ extends along the east edge of the White Sands Missile Range in a near north-south direction over a total length of 15,480 m(50,788 ft). For Mach 5 rain erosion tests, the sled operates on a monorail. Braking for these monorail sleds is accomplished by use of congealed water (colloidal silica) and waterfilled polyethylene bags or frangible plastic trays placed directly on the rail. Most rain erosion tests are conducted during the early morning hours (before dawn) to take advantage of the calm night air on the desert and to avoid collision with birds.

2. ROCKET SLEDS

Rocket sled hardware and motors were provided by the Holloman Test Track

Directorate. Satisfactory velocity profiles, with peak velocity occurring at the midpoint of the rainfield, were achieved for each test through proper selection of firing points, staging, and combinations of rocket propulsion units. The test vehicle assembly was mounted to the front of the sled assembly, as shown in *Figure C-1*.

3. INSTRUMENTATION

Sled velocity was measured by sensors positioned at regular intervals along the track. Photographic coverage included image motion compensation, horizontal shadowgraph, high-speed motion, and still documentary (before and after test).

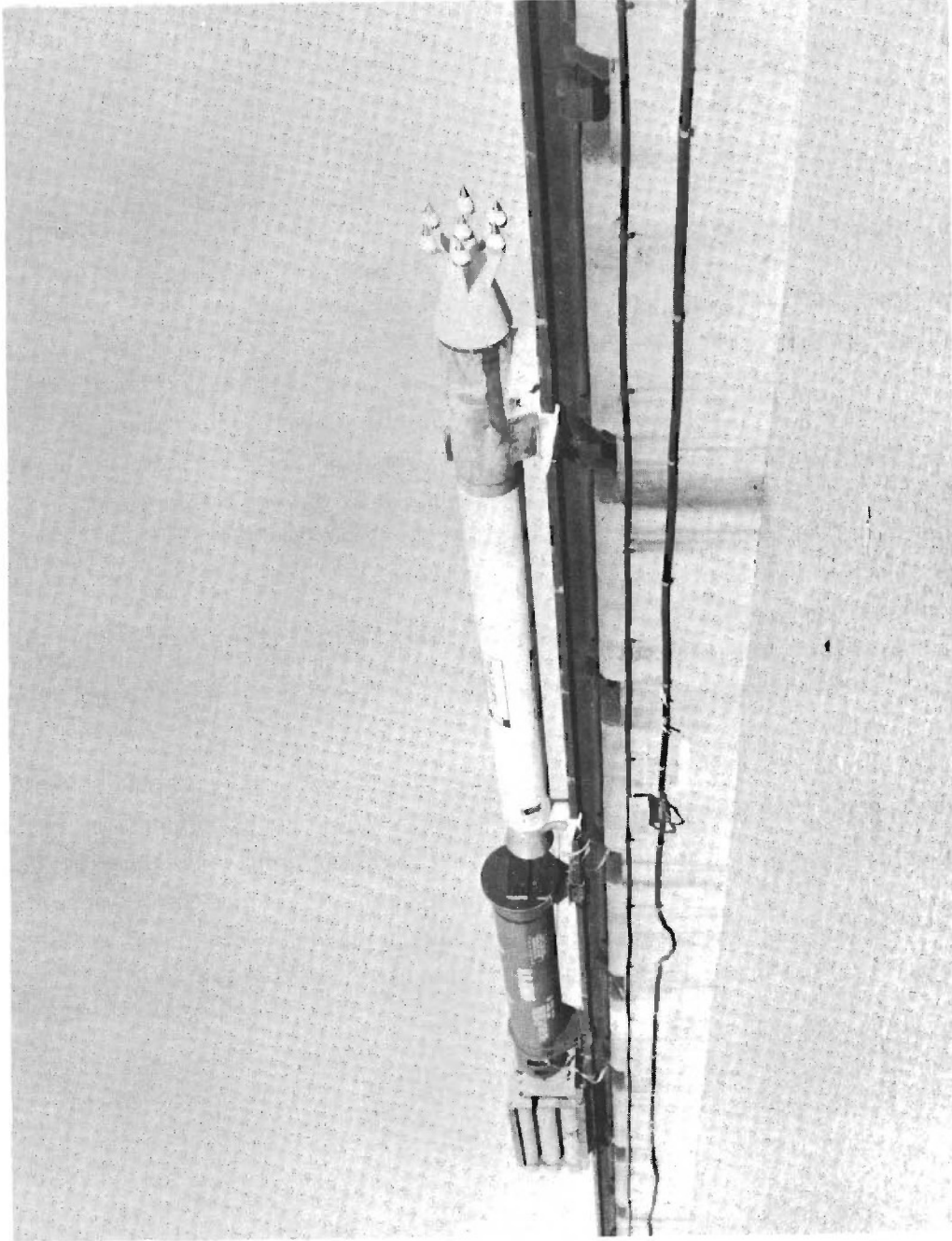


Figure C-1. Test vehicle and sled system.

APPENDIX D TEST ENVIRONMENT

1. RAINFIELD

The artificial rainfield (*Figure D-1*) at Holloman is supplied by spraying sections, 122 m (400 ft) in length, installed on the west side of the monorail. The spray heads are mounted on stand pipes and are located alternately 1.75 and 2.13 m (69 and 84 in.) above and 0.46 m (18.25 in.) west of the track at 1.2 m. (4 ft) intervals.

A nozzle pressure of 34.5 kPa (5 lb/in.²) provides a reasonably uniform rainfield with a density (mean liquid water content of the air) of 3.1 g/m³, a mean rain rate of 67 mm/hr (2.63 in./hr), and a mass median drop diameter of 1.37 mm.^{9,10} The drop size distribution is shown in *Figure D-2*. These calibration data were obtained without wind but are considered valid for cross-track winds that do not exceed 3 knots (1.55 m/sec) and in-track winds of 5 knots.

2. TRAJECTORY

It was decided that a velocity profile which peaked near the center of the rainfield would provide a profile flat enough for valid analysis. Nine trajectories for the tests are shown in *Figure D-3*. A summary of the sled test environment is found in *Table 2*.

3. AEROTHERMAL ENVIRONMENT AND TEMPERATURE EFFECTS

The calculated external surface temperature of a 15 deg SCFS sample reaches a maximum value of 950°C (1740°F) as shown in *Figure D-4* for the Mach 5 sled trajectory. At an angle of 22.5 deg the calculated maximum temperature is 1028°C (1822°F). The effect of rain on surface temperature was not included in the calculations.



Figure D-1. Holloman rainfield.

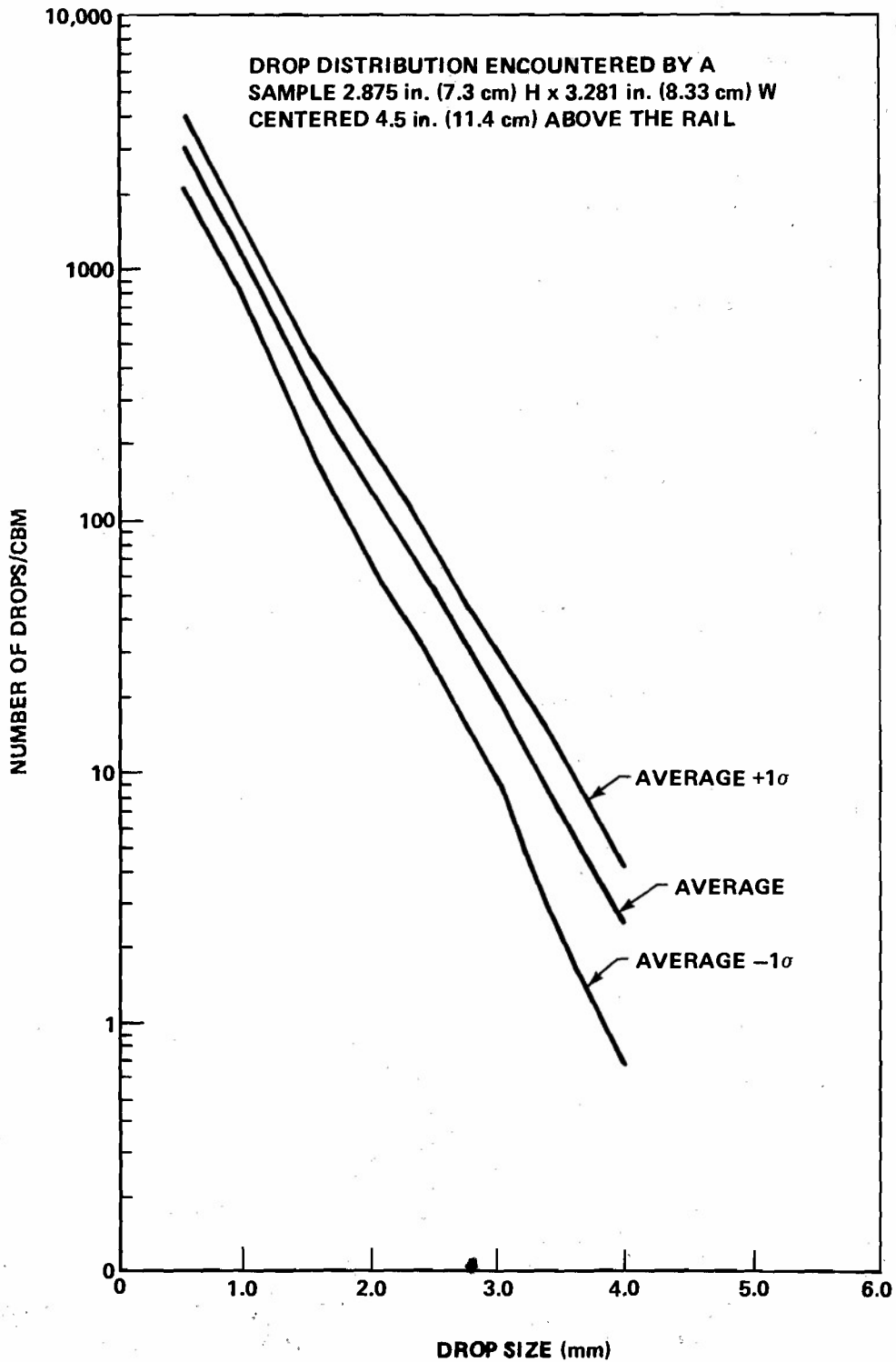


Figure D-2. Rainfield drop size distribution.

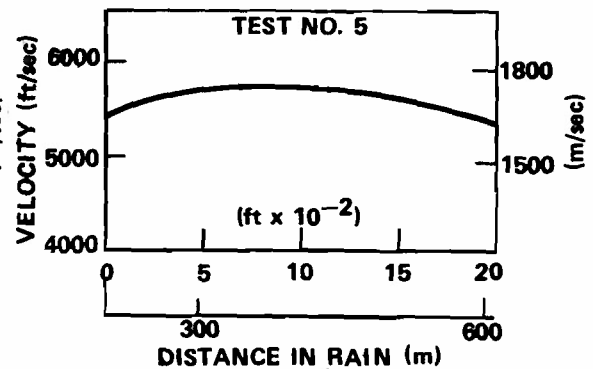
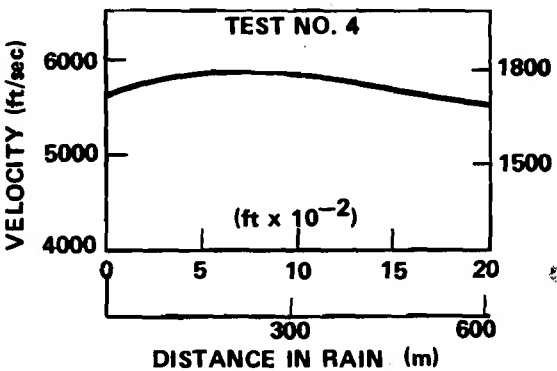
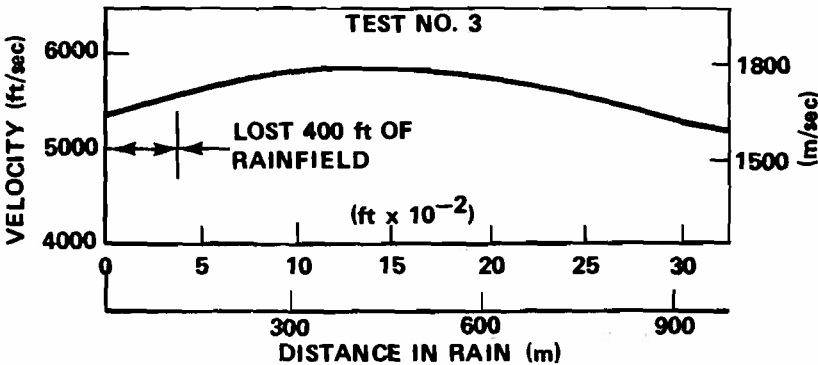
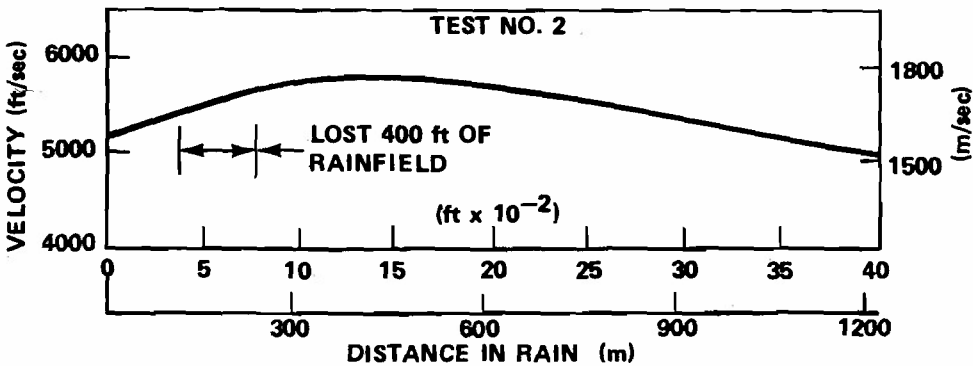
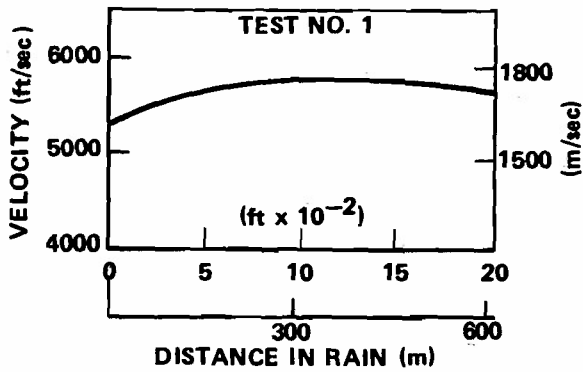


Figure D-3. Sled velocity in the rainfield.

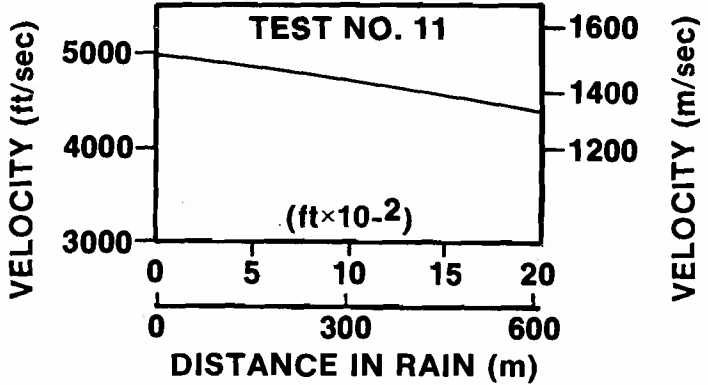
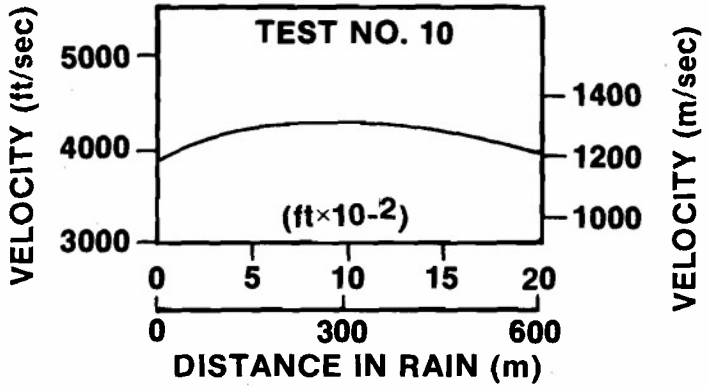
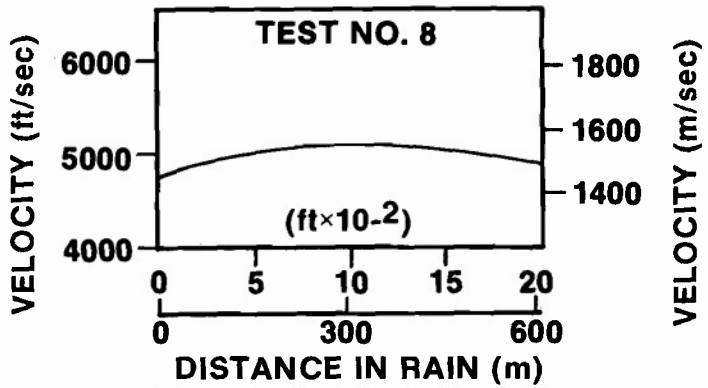
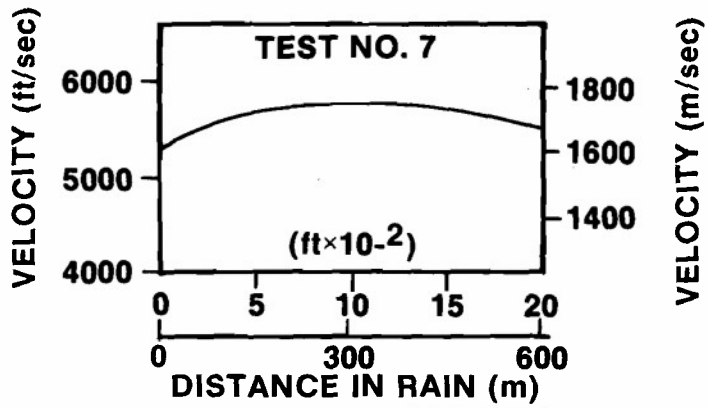


Figure D-3. (Concluded)

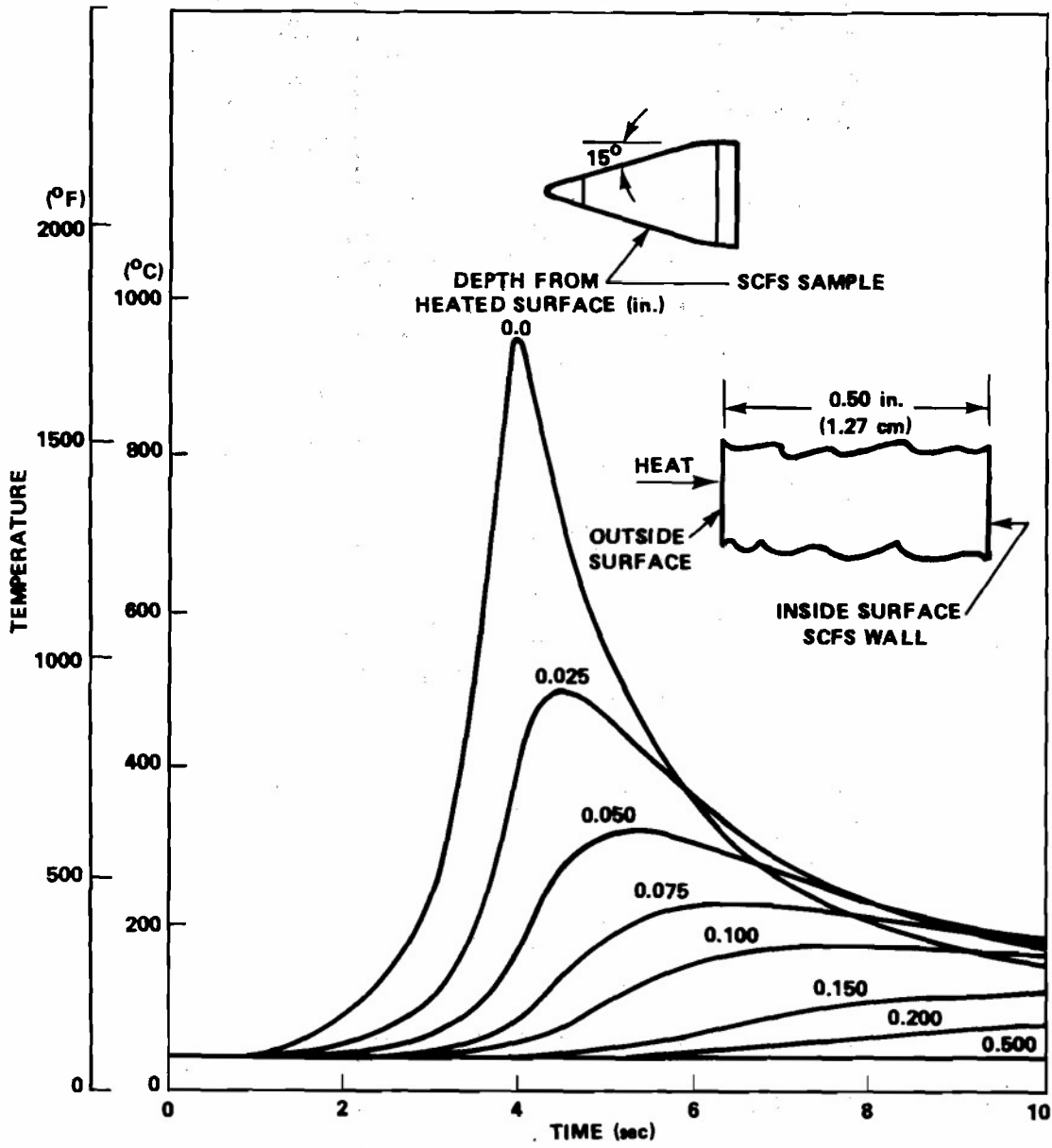


Figure D-4. Calculated temperature histories of SCFS in a Mach 5 sled test.

REFERENCES

1. Mueller, E. A., and Sims, A. L. *Measurement of the Simulated Rainfall at the Holloman Test Track Facility*, Prepared for Air Force Cambridge Research Laboratories, Bedford, Massachusetts, Final Report AFCRL-70-0282, April 1970.
2. Borough, C. K., *Determination of Criteria for Rain Erosion Testing of the Standard Arm Radome*, Part 1, General Considerations, Naval Weapons Center, Corona, California, NWCCCL TP 895, October 1969.
3. Harris, J. N.; Walton, J. D. Jr.; Johnson, B. E., et al., *Rain Erosion Sled Testing of Slip-Cast Fused Silica Radomes*, Final Technical Report, Project A-925, Contract DA-01-021-AMC 14464(2), Georgia Institute of Technology, Atlanta, Georgia, March 1967.
4. *Test and Evaluation Report, Rain Erosion Sled Tests (U)*, Raytheon Company Report No. BR-5351, June 1969 (Confidential).
5. Schmitt, G. F., *Rain Erosion Behavior of Materials at 5500 Feet per Second*, Air Force Materials Laboratory, Wright-Patterson Air Force Base, Ohio, Technical Report AFML-TR-72-64, 1972.
6. Walton, J. D., Jr., "State of Hypersonic Radome Technology Slip Cast Fused Silica and Reaction Sintered Silicon Nitride," Proceedings of the Third International Conference on Electromagnetic Windows, Paris, France, September 1975.
7. Letson, K. N., and Ormsby, P. A., *Rain Erosion Sled Tests of Radome Materials at Mach 5*, US Army Missile Command, Redstone Arsenal, Alabama, Report No. RL-76-19 (DDC Report No. AD-B012989L), 28 April 1976.
8. *The Holloman Track, Facilities and Capabilities*, Air Force Special Weapons Center, 6585th Test Group, Test Track Division, Holloman Air Force Base, New Mexico, 1974.
9. Engle, Berle, "Rainfield Calibration Data," (Private Communication), 6585th Test Group, Holloman Air Force Base, New Mexico, 29 August 1974.
10. Ehni, Friedrich P., *Layout and Calibration of the Rain Simulation at the Holloman Test Track*, 6585th Test Group (AFSC), Holloman Air Force Base, New Mexico, ADTC-TR-75-83, 15 November 1975.

DISTRIBUTION

	No. of Copies		No. of Copies
Defense Documentation Center Cameron Station Alexandria, Virginia 22314	12	Commander Naval Service Weapon Center NSWC-WOL, Code WA 21 ATTN: Mr. Bob Lucas White Oak, Maryland 20910	1
IIT Research Institute ATTN: GACIAC 10 West 35th Street Chicago, Illinois 60616	1	Martin-Marletta Corporation Orlando Division P. O. Box 5837 ATTN: Mr. G. Lively Mr. M. W. Garbrick Mr. E. A. Welsh Orlando, Florida 32805	1 2 1
Commander US Army Materiel Development and Readiness Command ATTN: DRCRD DRCDL 5001 Eisenhower Avenue Alexandria, Virginia 22333	1 1	Texas Instruments, Inc. ATTN: Dr. D. Purinton Dallas, Texas 75222	1
Commander Air Force Systems Command ATTN: Mr. George Schmitt, AFML/MBE Dr. Peter Land, AFML/LPO Dr. W. G. D. Frederick, AMFL/LPO Mr. John Koenig, AFML/LPO Mr. Donald J. Evans, AFML/LPJ Mr. Al Blume, AFAL/DHM-3 Wright Patterson Air Force Base, Ohio 45433	1 1 1 1 1 1	Hughes Aircraft ATTN: Mr. H. Leggett, MSD-133 Centinella and Teale Streets Culver City, California 90230	1
Commander 6585th Test Group, Test Track Division ATTN: TKG, Mr. Berie E. Engle TKE, Mr. Dan Krupovage TKT, Dr. Larry C. Mixon Holloman Air Force Base, New Mexico 88330	1 1 1	Rogers Corporation Lurie Research and Development Center ATTN: Mr. G. Robert Traut Rogers, Connecticut 06263	1
Director US Army Materials and Mechanics Research Center ATTN: DRXMR-RA, Dr. W.E. Davidsohn -EO, Dr. Robert N. Katz Mr. Fred Meyer Watertown, Massachusetts 02172	1 1 1	Rogers Corporation Micromat Division 85 Silverwood Road, NE ATTN: Mr. F. Stan Keahey Atlanta, Georgia 30342	1
Commander Naval Weapons Center Aerothermodynamics Branch (Code 4061) ATTN: Mr. C. F. Markarian China Lake, California	1	Applied Physics Laboratory The Johns Hopkins University ATTN: Dr. L. B. Weckesser Laurel, Maryland 20810	1
		Engineering Experiment Station Georgia Institute of Technology ATTN: Mr. J. D. Walton Mr. J. N. Harris Mr. H. L. Bassett 225 North Avenue, Northwest Atlanta, Georgia	1 1 1

	No. of Copies		No. of Copies
Rockwell International Missile Systems Division ATTN: Mr. Richard Wesley, MCDDO8 Anaheim, California 92803	1	Lockheed Missiles and Space Company, Inc. 3251 Hanover Street ATTN: Mr. W. H. Wheeler, Orgn. 52-31, Bldg. 102 Palo Alto, California 94304	1
Office of Naval Research ATTN: Dr. A. M. Diness, ONR 471 800 North Quincy Street Arlington, Virginia 22217	1	Brunswick Corporation 325 Brunswick Lane Marion, Virginia 24354	1
Raytheon Company Box M17-72-Hartwell Road ATTN: Mr. Kai Siwiak Mr. William House Bedford, Massachusetts 01730	1 1	Hughes Aircraft Company, Missile Systems Group 8433 Fallbrook Avenue ATTN: Mr. Denis Quan Mr. Robert D. Nielsen Canoga Park, California 91304	1 1
Raytheon Company, Research Division 28 Seyon Street ATTN: Mr. J. Stanley Waugh Waltham, Massachusetts 02154	1	Flight Systems, Inc. P. O. Box 2400 ATTN: Mr. Bernard Crowe Newport Beach, California 92663	1
General Dynamics Corporation P. O. Box 2507 ATTN: Mr. John H. Rizley Pomona, California 91766	1	Tennessee Technological University Department of Engineering Science ATTN: Dr. Joseph Scardina Cookeville, Tennessee 38501	2
General Dynamics/Electronics Division P. O. Box 81127 ATTN: Mr. Armando Mendez, Mail Zone 761 San Diego, California 92138	1	US Army Materiel Systems Analysis Activity ATTN: DRXSY-MP Aberdeen Proving Ground, Maryland 21005	1
Battelle Columbus Laboratories 505 King Avenue ATTN: Mr. Roger R. Willis Columbus, Ohio 43201	1	ONERA 29 rue de la Division Leclerc ATTN: Mr. D. L. Balageas Chatillon sous Bagneux, France 92320	1
McDonnell Douglas Astronautics Company P. O. Box 516 St. Louis, Missouri 63166	1	Lockheed Missiles and Space Company, Inc. 4800 Bradford Drive NW ATTN: Mr. S. J. Robertson Huntsville, Alabama 35806	1
The Boeing Company P. O. Box 3999 Seattle, Washington 98124	1	Commander Naval Air Systems Command AIR-5052 ATTN: Mr. C. F. Bersch Mr. M. Stander Washington, D. C. 20361	1 1
AVCO Corporation/Systems Division 201 Lowell Street ATTN: Mr. Frank Tempesta Wilmington, Massachusetts 01887	1	Commander ADTC/AFATL/DLMI ATTN: Mr. J. B. Oliphint Mr. C. Butler Eglin Air Force Base, Florida 32542	1 1
Northrop Corporation 3901 W. Broadway 3544/83 ATTN: Mr. Allan B. Hitterdal Hawthorne, California 91364	1		

	No. of Copies		No. of Copies
Sandia Laboratories		-TG	1
ATTN: Mr. Stanley Meyer	1	-TGN, Mr. J. McLean	1
Organization 4342		-TGT	1
Albuquerque, New Mexico 87185		-TL	2
		-TLA, Mr. K. N. Letson	12
		-TLA	1
DRCPM-HA	1	-E	1
-HAE, Mr. W. Moore	1	-EAM, Mr. P. Ormsby	3
-MDE, Mr. G. Nicholas	1	-EAM, Mr. E. Verchot	1
-PE-E, Mr. J. Pemberton	1	-ES	1
Mr. J. Pettitt	1	-ET	1
-ROL-E	1	-N	1
-RS, Mr. B. Richardson	1	-TR	1
DRSMI-LP, Mr. Voigt	1	-TT	1
DRDM-X	1	-TBD	3
-T, Dr. Kobler	1	-TI (Record Set)	1
-CD, Mr. T. Morgan	1	(Reference Copy)	1
-Y	1		
-YT, Mr. J. W. Hooie	1		
-TC	1	US Army Materiel Systems	
-TDK, Mr. R. Deep	1	Analysis Activity	
-TE	1	ATTN: DRXSY-MP	1
-TER, Mr. R. Russell	1	Aberdeen Proving Ground, Maryland 21005	